ISTerre
Institut des Sciences de la Terre

European Research Council
Adv. Grant Whisper

Introduction to passive imaging and monitoring in seismology

Material from the chapter « Noise correlations » by Campillo and Roux, Treatise of Geophysics 2013

Michel Campillo,
ISTerre
Université Joseph Fourier and CNRS,38041 Grenoble, France

Cargèse 2013

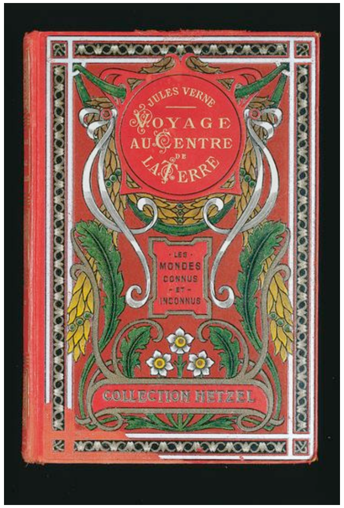

-Introduction

-Passive imaging

-Monitoring the changing Earth

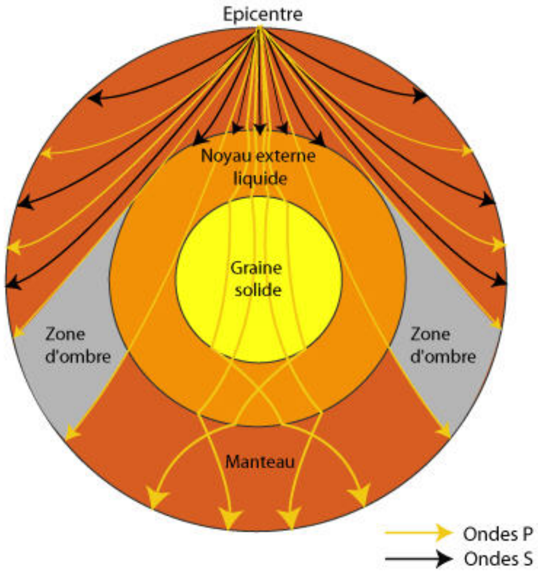

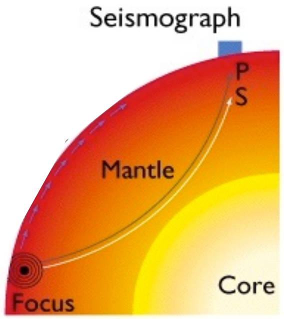

Seismograms recorded at a distance of 110°, showing surface waves.

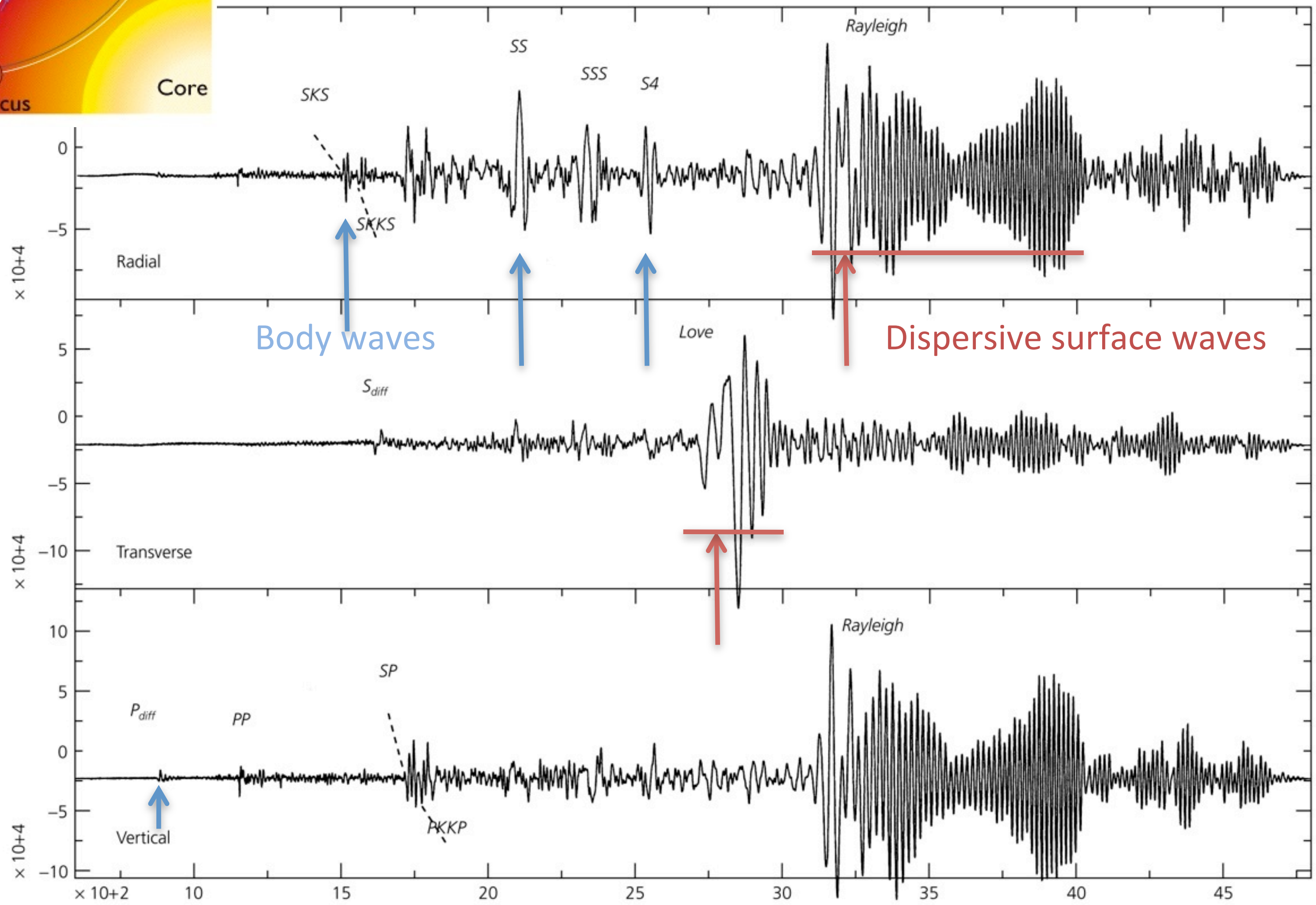

From Stein and Wysession

Figure 1.2-1: Global seismicity, 1963-1995.

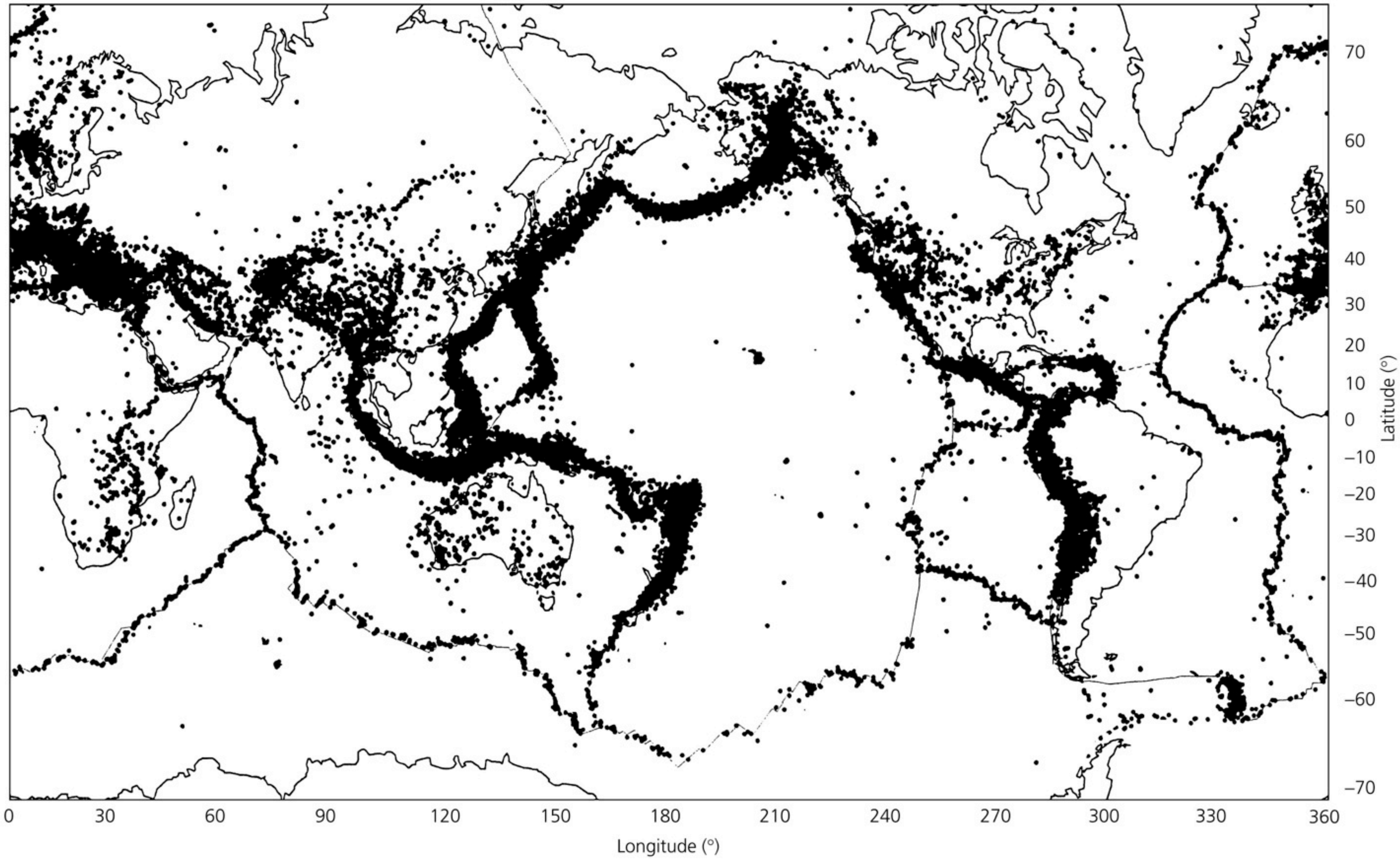

Une journée AVEC un grand séisme

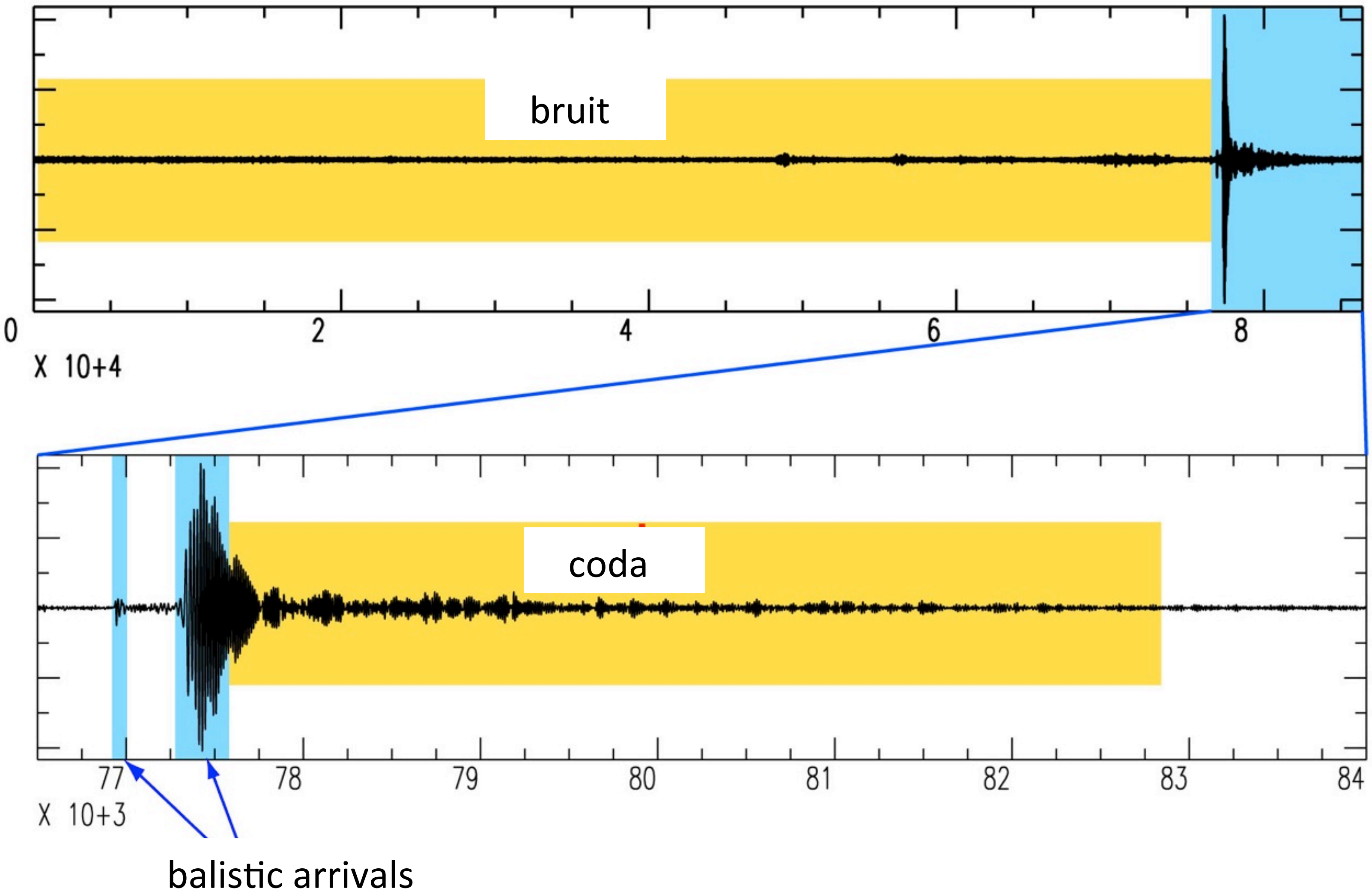

The coda is the result of multiple scattering

Large networks – continuous recordings

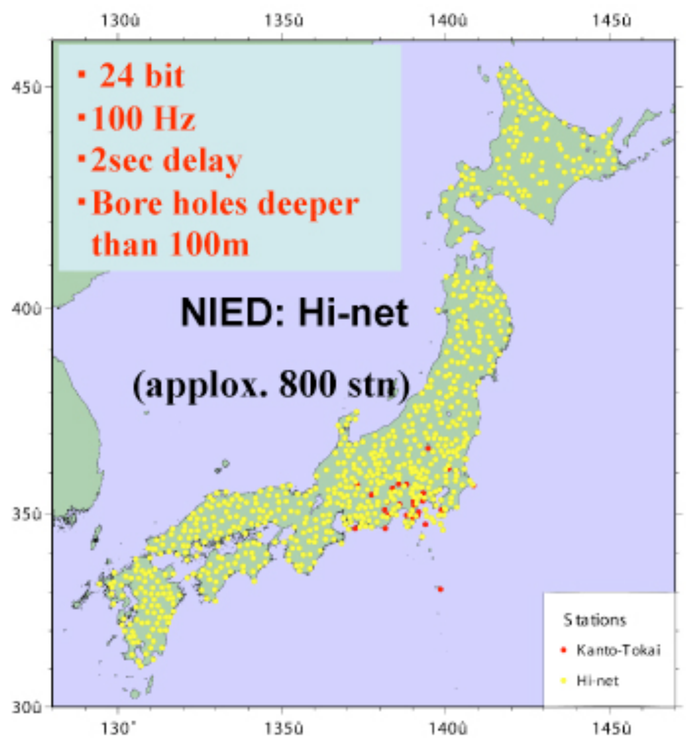

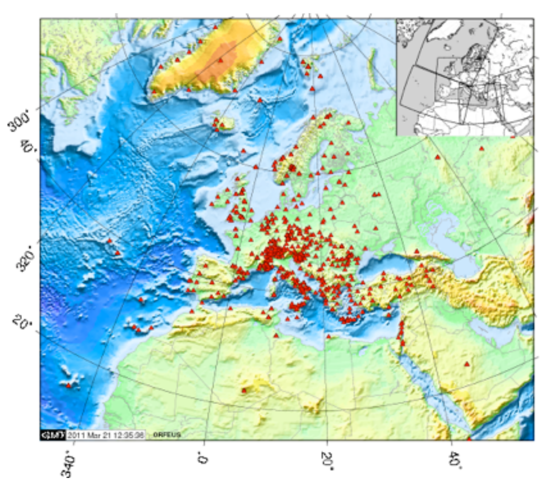

Seismology : huge data sets consisting for a large part of 'ambient noise'..

Exploration data and more : J. Meunier

Global ‘noise’ sources in the microseism band
(extended ≈2-50s)

Strong contribution from oceanic waves

Example of a global comparison

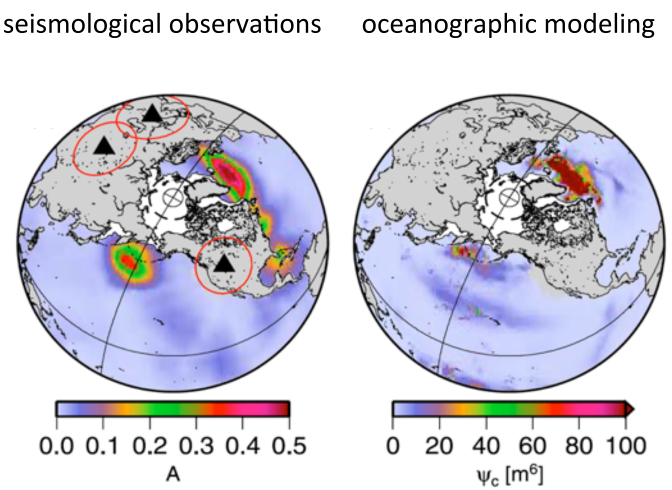

Hillers et al., 2012

(*presentation by F. Ardhuin*)

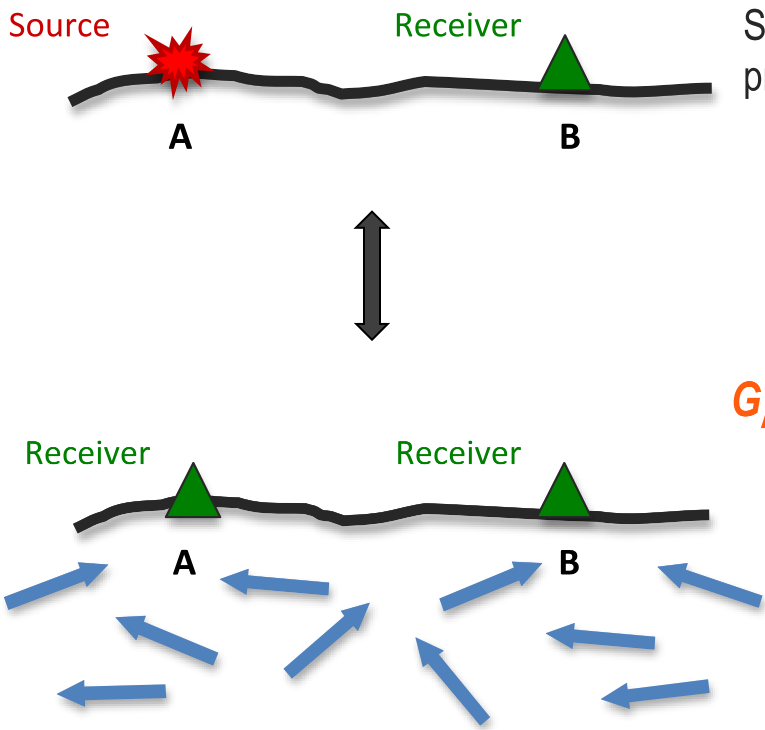

Source in A $\Rightarrow$ the signal recorded in B characterizes the propagation between A and B.

➡ **Green function** between A and B: G_{AB}

G_{AB} can be reconstructed by the correlation of noise or « diffuse » (equipartitioned) fields recorded at A and B (C_{AB})

Experimentally verified with seismological data (Campillo and Paul, 2003; Shapiro and Campillo, 2004,……..)

Definitions

-Crosscorrelation of the signals $u_1(t)$ at $\vec{r}_1$ and $u_2(t)$ at $\vec{r}_2$

$$C(\vec{r}_1, \vec{r}_2; t) = C_{1,2}(t) = \frac{1}{T}\int_0^T u_1(\tau) u_2(t+\tau)\, d\tau$$

and in the frequency domain: $C(\vec{r}_1, \vec{r}_2; \omega) = C_{1,2}(\omega) = u_1(\omega) u_2^*(\omega)$

-Green function (source at origin):

$$\Delta G(\vec{x}; t) - \frac{1}{c^2}\frac{\partial G(\vec{x}; t)}{\partial t^2} = \delta(\vec{x})\delta(t)$$

-Causality and Fourier transform:

$$\mathrm{Im}(G(\omega)) = \frac{1}{2i}(G(\omega) - G^*(\omega))$$

$$TF(i\,\mathrm{Im}(G(\omega))) = \frac{1}{2}(G(t) - G(-t))$$

Causality: the example of the 2D scalar Green function

$$G(\omega) = \frac{1}{4\mathrm{i}\mu} H_0^{(2)}\left(\frac{\omega r}{\beta}\right)$$

$$G(t) = \frac{1}{2\pi\mu} \frac{H\left(t - r/\beta\right)}{\sqrt{t^2 - r^2/\beta^2}}$$

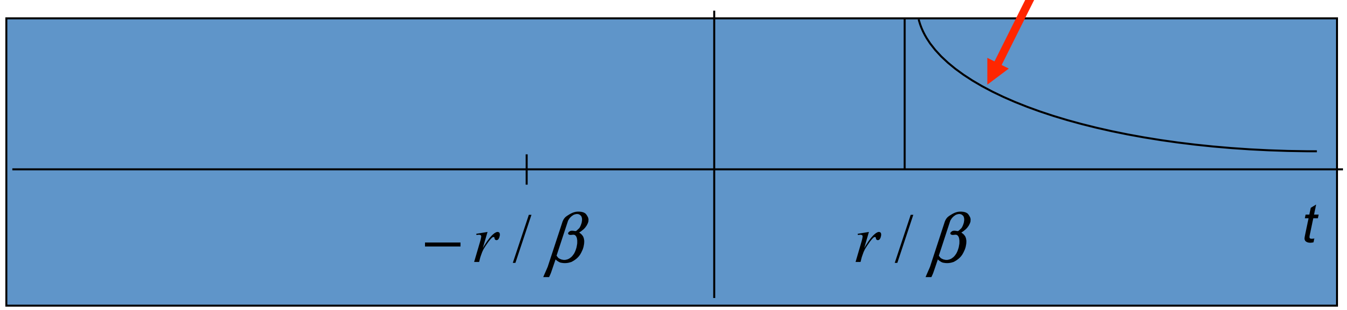

G/2

FT(Re(G))

FT(i Im(G))

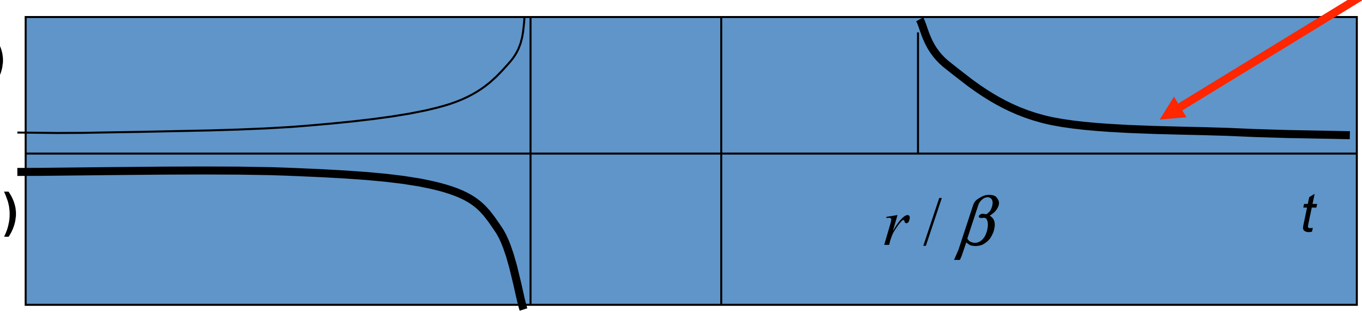

$$TF(i\,\mathrm{Im}(G(\omega))) = \frac{1}{2}(G(t) - G(-t))$$

Arbitrary medium: an integral representation written in the frequency domain

(see e.g. Weaver et al. 2004, or Snieder, 2007)

$$G_{12} - G_{12}^{*} = \frac{4i\omega\kappa}{c}\int_{\mathcal{V}} G_{1x} G_{2x}^{*}\, dV + \oint_{S} \left[G_{1x} \vec{\nabla}\left(G_{2x}^{*}\right) - \vec{\nabla}\left(G_{1x}\right) G_{2x}^{*} \right] \overrightarrow{dS}$$

Volume term

Surface term

FT of *G(-t)*

Absorption coefficient

FT of *G(t)*

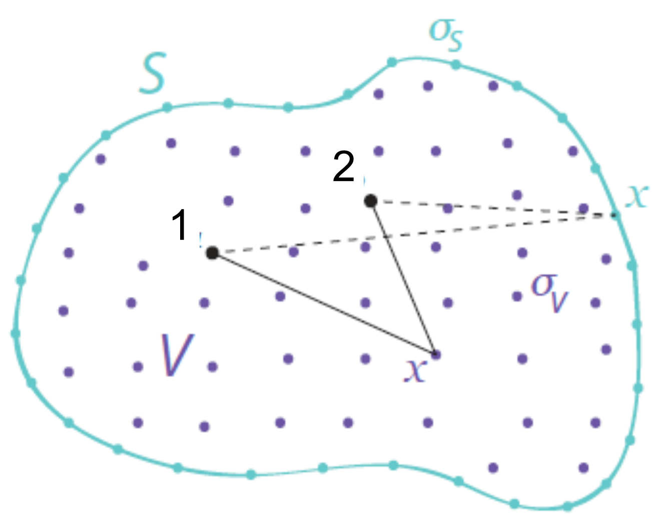

Helmholtz equation $G_{1x} = G(\vec{r}_1, \vec{x}; \omega)$

$$\Delta G_{1x} + V(\vec{x}) G_{1x} + (k + i\kappa)^2 G_{1x} = \delta(\vec{x} - \vec{r}_1)$$

where the potential $V(\vec{x})$ describes the scattering contribution does not extend to infinity.

As for the classical representation theorem, we consider a combination of the fields from source at 1 and 2 and compute the flux:

$$I = \oint_S \left[G_{1x} \vec{\nabla}\left(G_{2x}^*\right) - \vec{\nabla}\left(G_{2x}\right) G_{1x}^* \right] \overrightarrow{dS}$$

With the divergence theorem:

$$I = \int_{\mathcal{V}} \vec{\nabla} \left[G_{1x} \vec{\nabla}\left(G_{2x}^*\right) - \vec{\nabla}\left(G_{1x}\right) G_{2x}^* \right] dV$$

$$I = \int_{\mathcal{V}} \vec{\nabla}\left[G_{1x} \vec{\nabla}\left(G_{2x}^{*} \right) - \vec{\nabla}\left(G_{1x} \right) G_{2x}^{*} \right] dV$$

reduces to

$$I = \int_{\mathcal{V}} \left(G_{1x} \Delta G_{2x}^{*} - \Delta G_{1x} G_{2x}^{*} \right) dV$$

Using the definition of the GF:

$$\Delta G_{1x} = \delta\left(\vec{x} - \vec{r}_1 \right) - V\left(\vec{x} \right) G_{1x} - \left(k + i\kappa \right)^2 G_{1x}$$

we obtain:

$$I = G_{12} - G_{21}^{*} - \frac{4i\omega\kappa}{c} \int_{\mathcal{V}} G_{1x} G_{2x}^{*} \, dV$$

and finally:

$$G_{12} - G_{12}^{*} = \frac{4i\omega\kappa}{c} \int_{\mathcal{V}} G_{1x} G_{2x}^{*} \, dV + \oint_{S} \left[G_{1x} \vec{\nabla}\left(G_{2x}^{*} \right) - \vec{\nabla}\left(G_{1x} \right) G_{2x}^{*} \right] \overrightarrow{dS}$$

Surface term: $$G_{12} - G_{12}^{*} = \oint_S \left[G_{1x} \vec{\nabla}\left(G_{2x}^{*}\right) - \vec{\nabla}\left(G_{1x}\right) G_{2x}^{*} \right] \overrightarrow{dS}$$

κ =0 (no attenuation)

No source in the bulk

Surface term:

$$G_{12} - G_{12}^{*} = \oint_{S} \left[G_{1x} \vec{\nabla} \left(G_{2x}^{*} \right) - \vec{\nabla} \left(G_{1x} \right) G_{2x}^{*} \right] \overrightarrow{dS}$$

If the surface is taken in the far field of the medium heterogeneities

$$G_{1x} \sim \frac{1}{4\pi \left| \vec{x} - \vec{r}_1 \right|} \exp\left(-ik \left| \vec{x} - \vec{r}_1 \right| \right) \text{ and } \vec{\nabla}\left(G_{1x} \right) \sim i\vec{k}\, G_{1x}$$

and we obtain another widely used integral relation:

$$G_{12} - G_{12}^{*} = -2i \frac{\omega}{c} \oint_{S} G_{1x} G_{2x}^{*} \, dS$$

Talk by A. Curtis on integral representations and applications

Volume term: $$G_{12} - G_{12}^{*} = \frac{4i\omega\kappa}{c} \int_{\mathcal{V}} G_{1x} G_{2x}^{*} \, dV$$

κ is finite (attenuation)

S is assumed to be sufficiently far away, for its contribution to be neglected (spreading and attenuation)

An homogeneous infinite body with an even random distribution of sources

Green function

$$G(\vec{r}_1,\vec{r}_2;t)=\frac{1}{2\pi}\int_{-\infty}^{+\infty}d\omega\frac{1}{4\pi|\vec{r}_2-\vec{r}_1|}\exp\left[i\omega\left(t-\frac{|\vec{r}_2-\vec{r}_1|}{c}\right)\right]\exp\left(-\kappa|\vec{r}_2-\vec{r}_1|\right)$$

Contribution from
Random sources

$$P(\vec{r}_1;t)=\int_{-\infty}^{\infty}\int_{-\infty}^{t}d\vec{x}\,dt_x S(\vec{x},t_x)G(\vec{r}_1,\vec{x};t-t_x)$$

$$\langle S(\vec{x},t_x)S(\vec{x}',t_{x'})\rangle=Q^2\delta(t_x-t_{x'})\delta(\vec{x}-\vec{x}')$$

Correlation with finite duration

$$C(\vec{r}_1,\vec{r}_2;t)=C_{1,2}(t)=\frac{1}{T}\int_0^T P(\vec{r}_1;\tau)P(\vec{r}_2;t+\tau)d\tau$$

$$\frac{d}{dt}\langle C_{1,2}(t)\rangle=Q^2N\frac{c}{2\kappa}\left[G(\vec{r}_1,\vec{r}_2;t)-G(\vec{r}_1,\vec{r}_2;-t)\right]$$

with Q^2N being the noise power during T

<time derivative of correlation> ≈ causal+acausal Green functions

Location of the sources that contribute to the correlation: the end fire lobes

Difference of travel time between A and B
wrt the position of the source

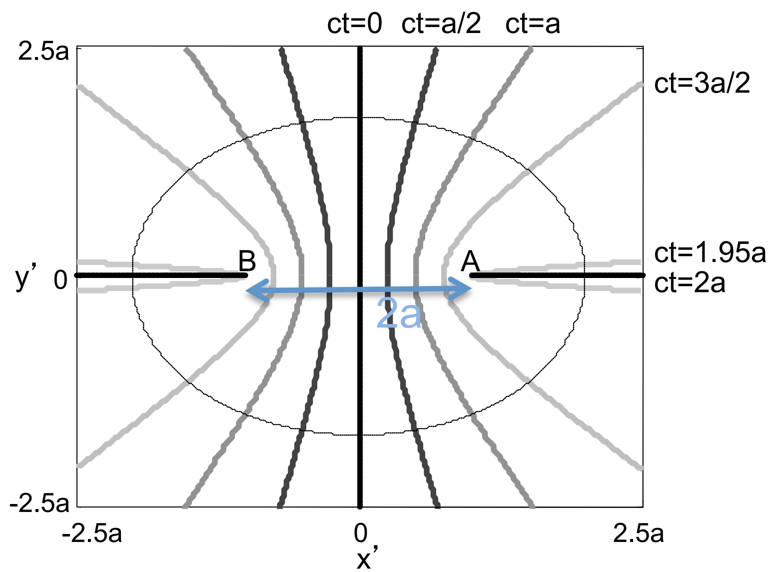

Stationary phase and end fire lobes

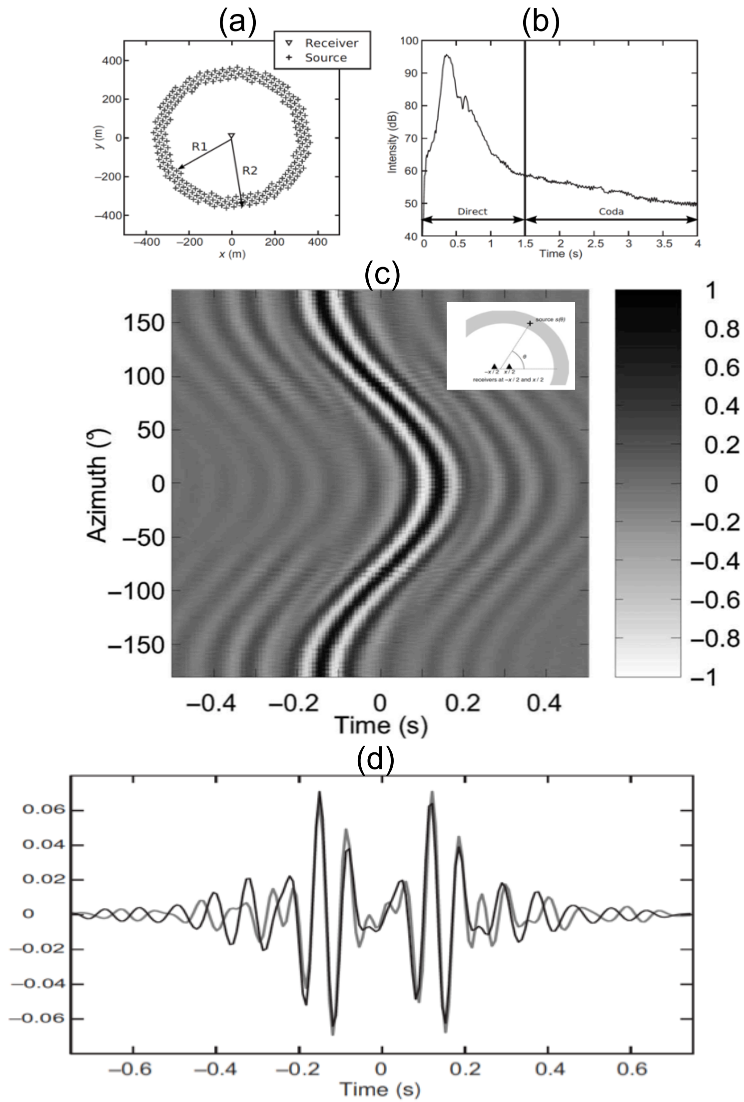

From Gouédard et al., 200X

End fire lobes

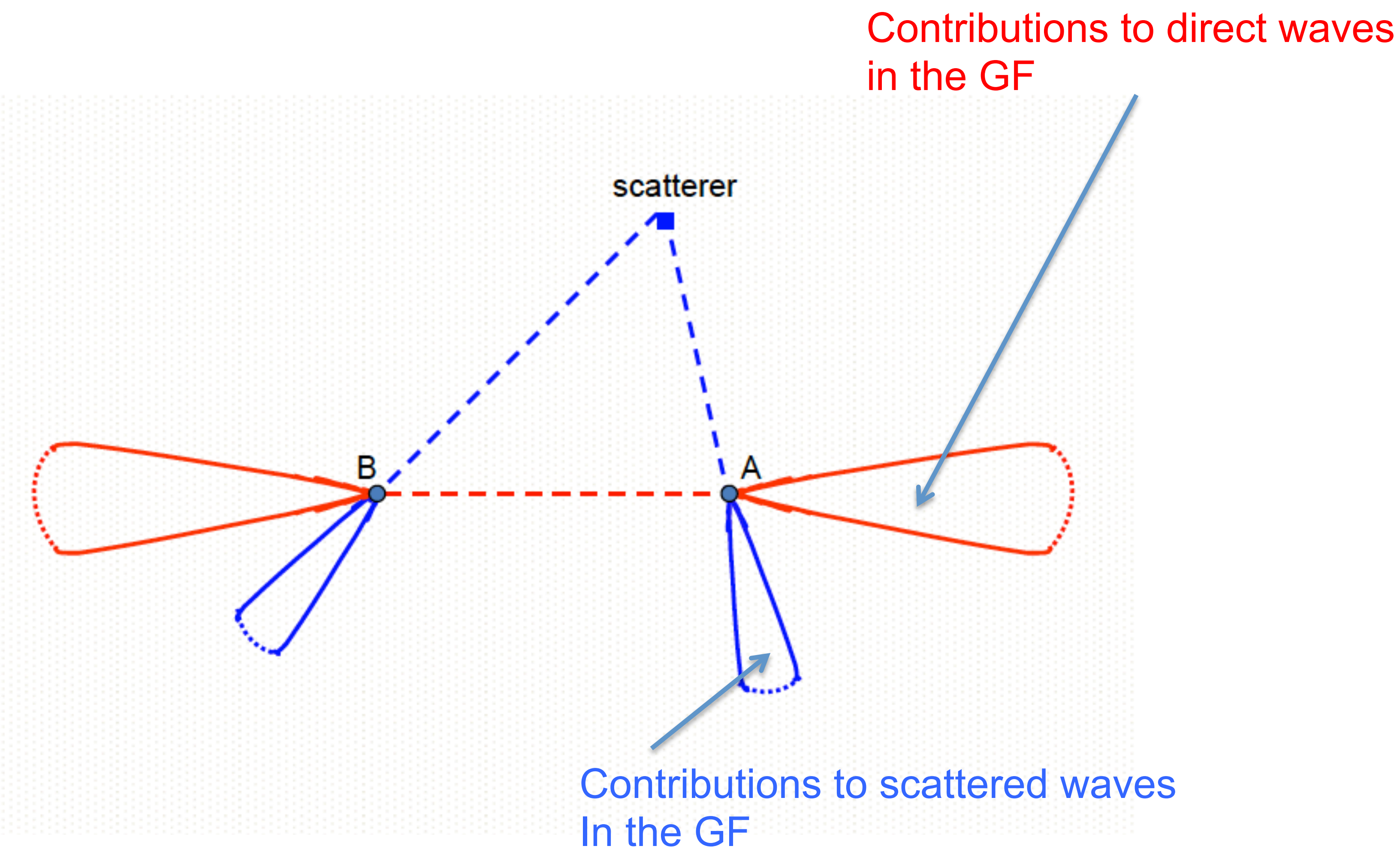

Extension to scattered waves

Talks by H. Sato and J. Garnier

In practice, the noise sources are not evenly distributed and the field is not equipartitioned.

At first order we can study the effect of non isotropy of the field incident on the receivers.

It results in bias on the measurements of direct path travel times.

Increasing anisotropy of the noise intensity *B*

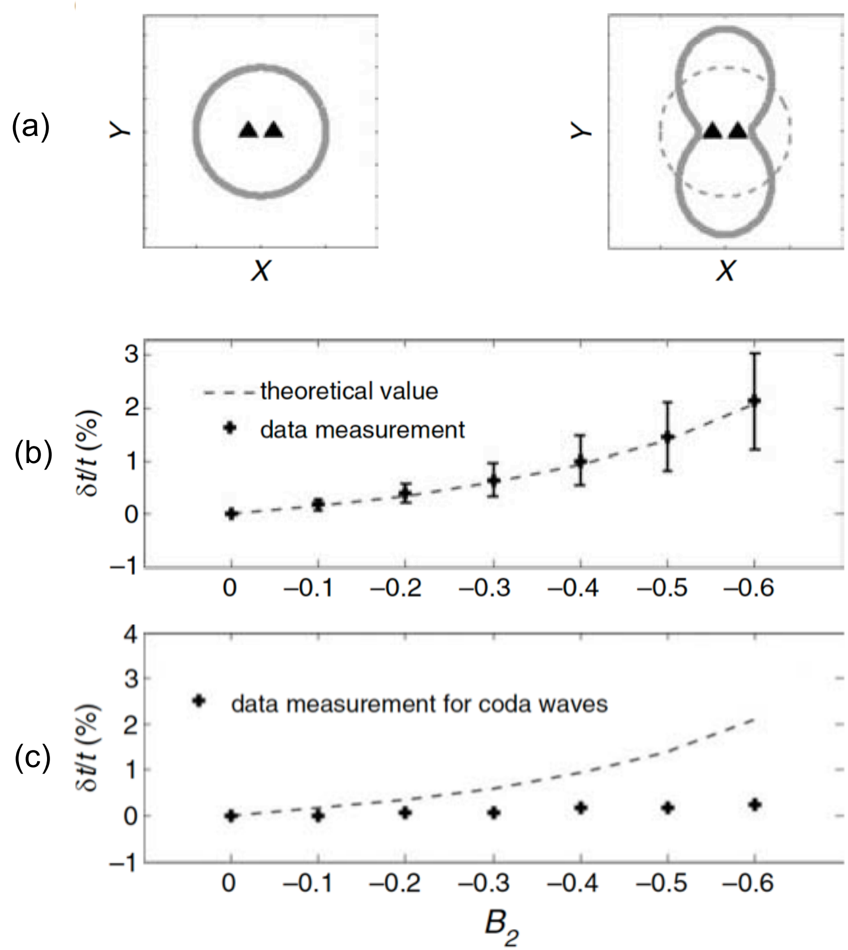

$$B(\theta) = 1 + B_2 \cos(2\theta)$$

Bias in the correlation of direct waves

Bias in the correlation of coda waves

From Froment et al., 2011.

Multiple scattering and equipartition

Equipartion principle for a completely randomized (diffuse) wave-field: in average, all the modes of propagation are excited to equal energy.

Implication for diffuse elastic waves *(Weaver, 1982, Ryzhik et al., 1996)*: P to S energy ratio stabilizes at a value independant of the details of scattering.

Numerical simulation *(Margerin et al.2000)*

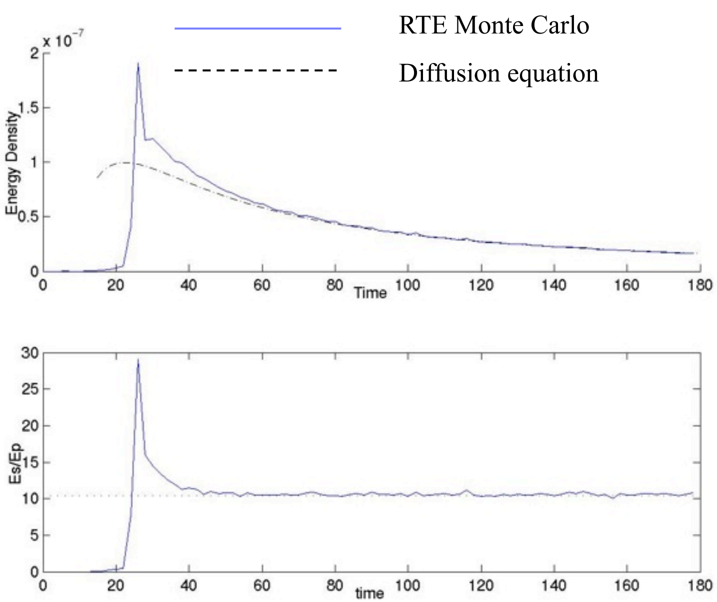

Observations *(Hennino et al., 2001)*

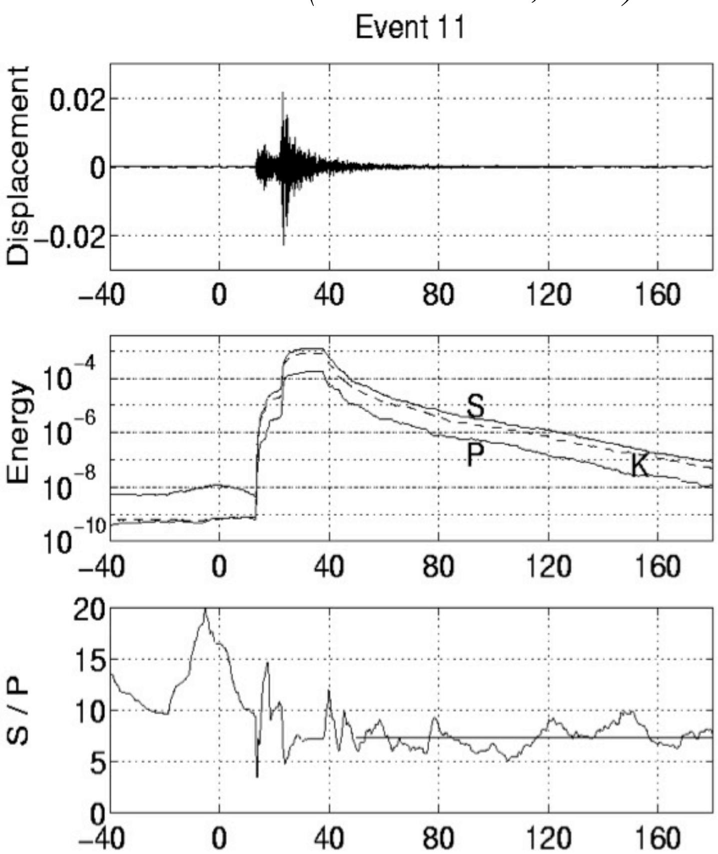

Multiple scattering and equipartition (finite body)

equipartion

$$\phi(\vec{r};t) = \sum_n a_n U_n(\vec{r}) \cos(\omega_n t)$$

$$< a_n a_m^* >= F(\omega_n)\delta_{nm}$$

correlation

$$C_{1,2}(t) = \frac{1}{T}\int_0^T \phi(\vec{r}_1,\tau)\phi(\vec{r}_2,t+\tau)d\tau$$

Assuming a long recording interval T, this reduces to:

$$C_{1,2}(t) = \frac{1}{2}\sum_n F(\omega_n) U_n(\vec{r}_1) U_n(\vec{r}_2) \cos(\omega_n t)$$

Compare with:

$$G(\vec{r}_1,\vec{r}_2;t) = \sum_n U_n(\vec{r}_1) U_n(\vec{r}_2) \frac{\sin(\omega_n t)}{\omega_n} \Theta(t)$$

1 derivative 2 causality

The ‘correlation relation’ (under the hypothesis of random sources or multiple scattering):

$$\partial_\tau C_{AB}(\tau) \propto G^+(A,B,\tau) - G^-(A,B,-\tau)$$

Correlation of fields in A and B

Green function between A and B (for positive and negative times)

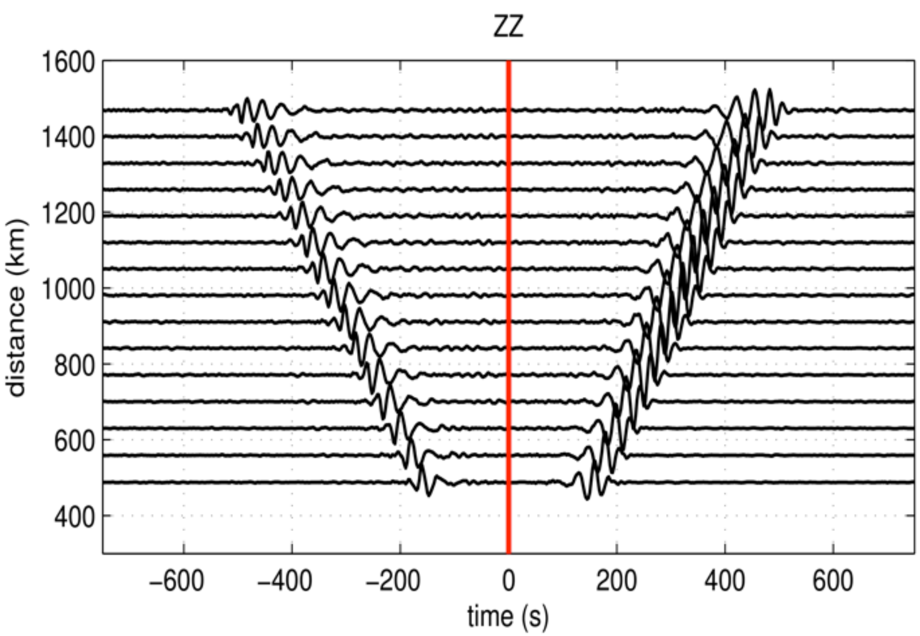

Rayleigh waves across USArray (from P. Boué, UJF)

Superposition of G(t) and G(-t)…….

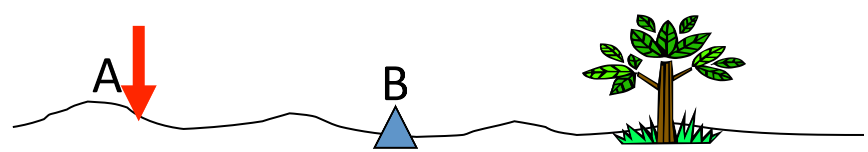

-Introduction

-**Passive Imaging**

-Suivre les évolutions de la terre solide

Surface wave imaging with seismic noise….. it works

Map of Rayleigh group velocity Vg
(linear inversion)

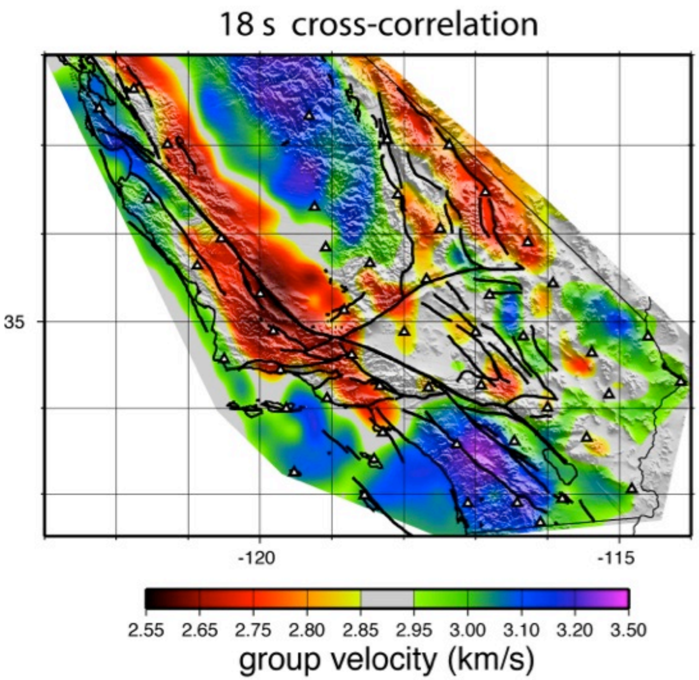

Shapiro et al. Science 2005.

3D shear velocity model

1) Vg(x,y,T)
2) Vs(x,y,z) local non linear inversion

The Moho beneath the Alps

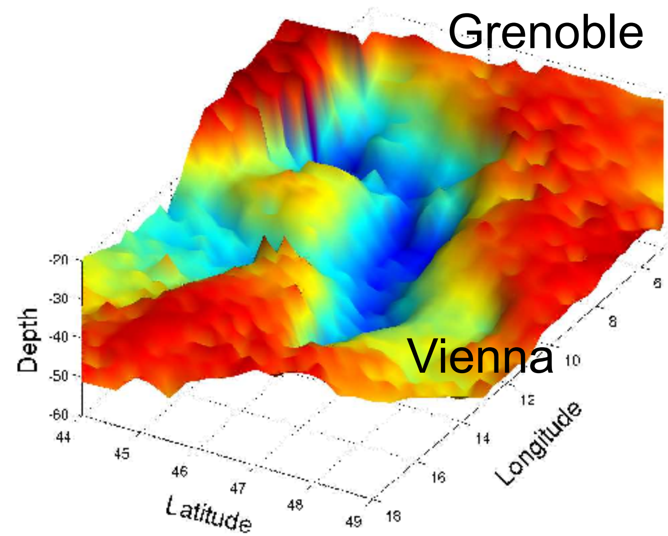

Stehly et al. ,2009

Refined imaging within a large array

(*Pierre Boué 2013)*

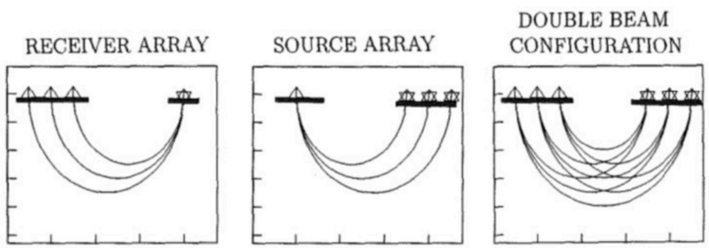

Weber et al., 1996

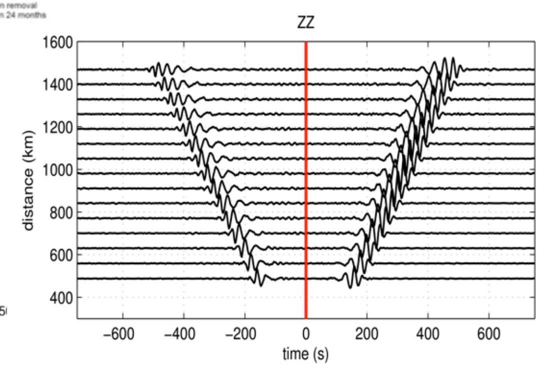

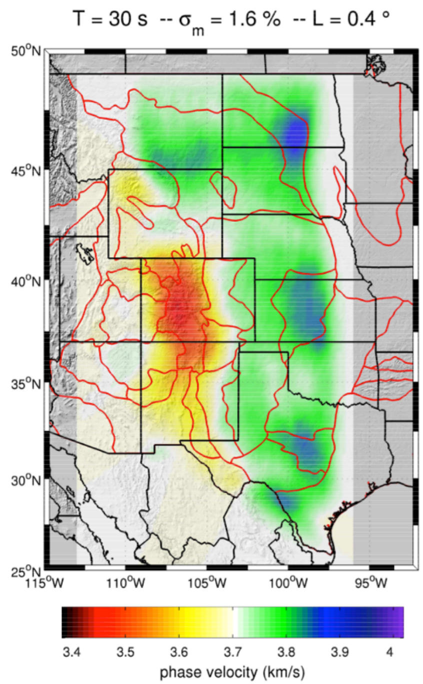

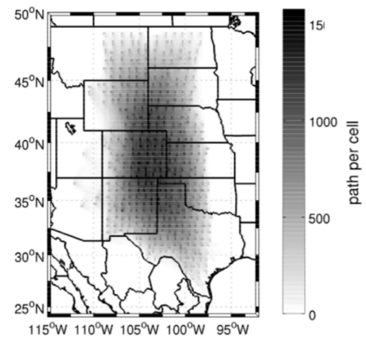

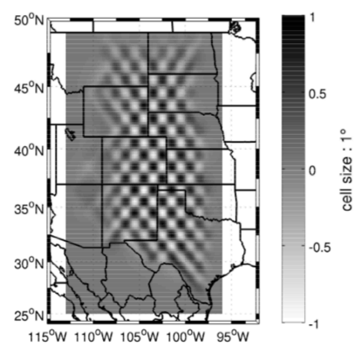

With ray bending

Presentations by R. van der Hilst and G. Prieto

Surface wave tomography ➔ body waves (deep reflections)

Comparison of high frequency (1Hz) 1-year noise correlation with earthquake data

Poli et al. 2012a

POLENET/LAPNET array in Finland

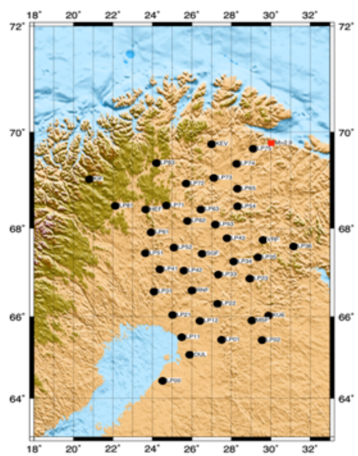

Z-Z noise correlations

Z comp. actual earthquake

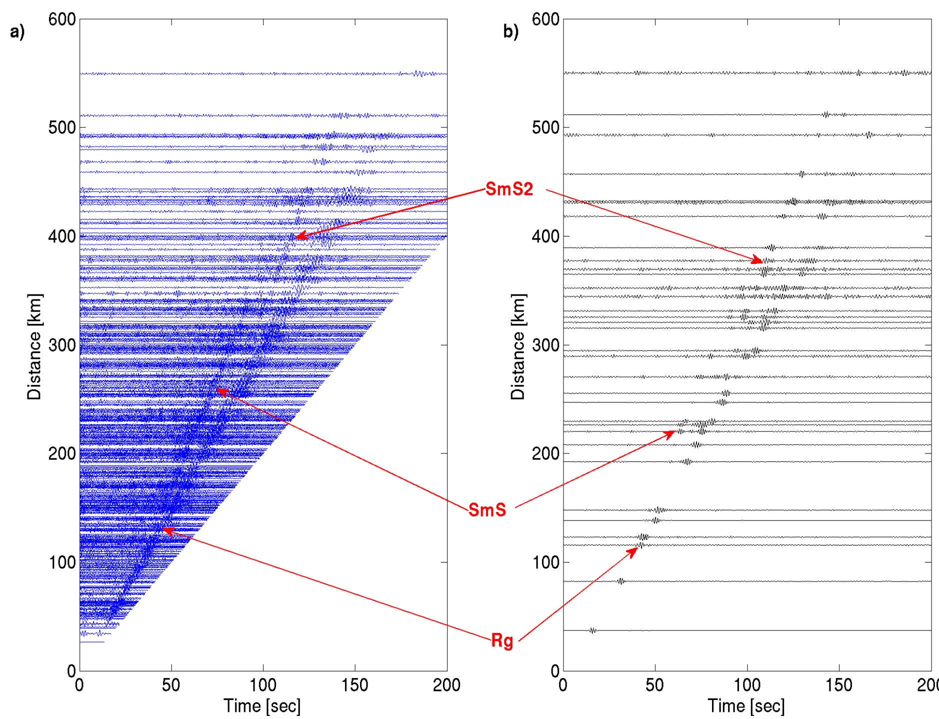

Comparison with synthetic Green functions

C_{ZZ} (data) GF_{ZZ} (theory) C_{RR} (data) GF_{RR} (theory)

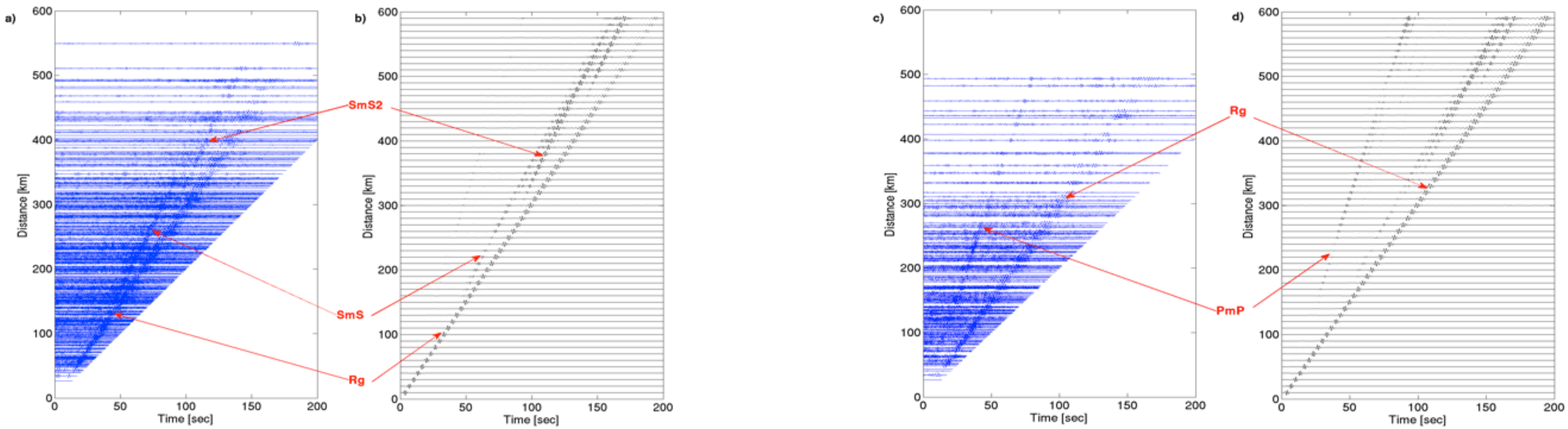

Reconstruction of P and S multiple reflections

Polarisation: noise correlation vs synthetics

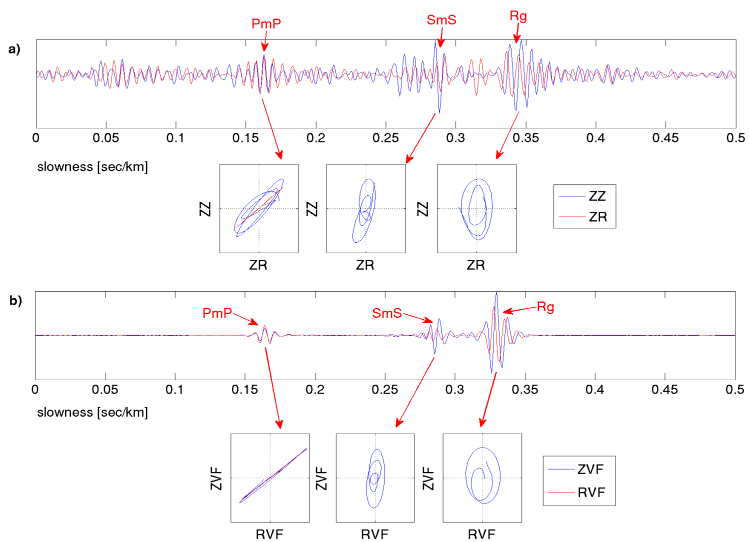

Good reconstruction of phase and relative amplitudes of the components of the reflected waves. (amplitude discussed by Prieto)

A favorable context: distance vs. mean free path, amplitude in actual earthquake records

➔ Deep phases

Poli et al., 2012a

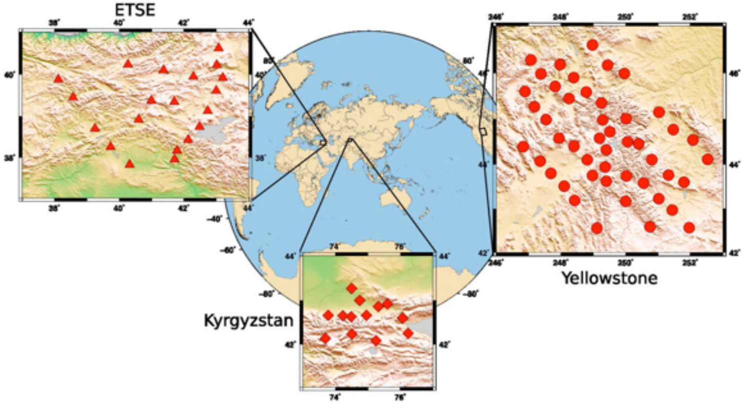

Ambient noise Array analysis

Landès et al., 2010

High apparent velocity arrivals: deep phases

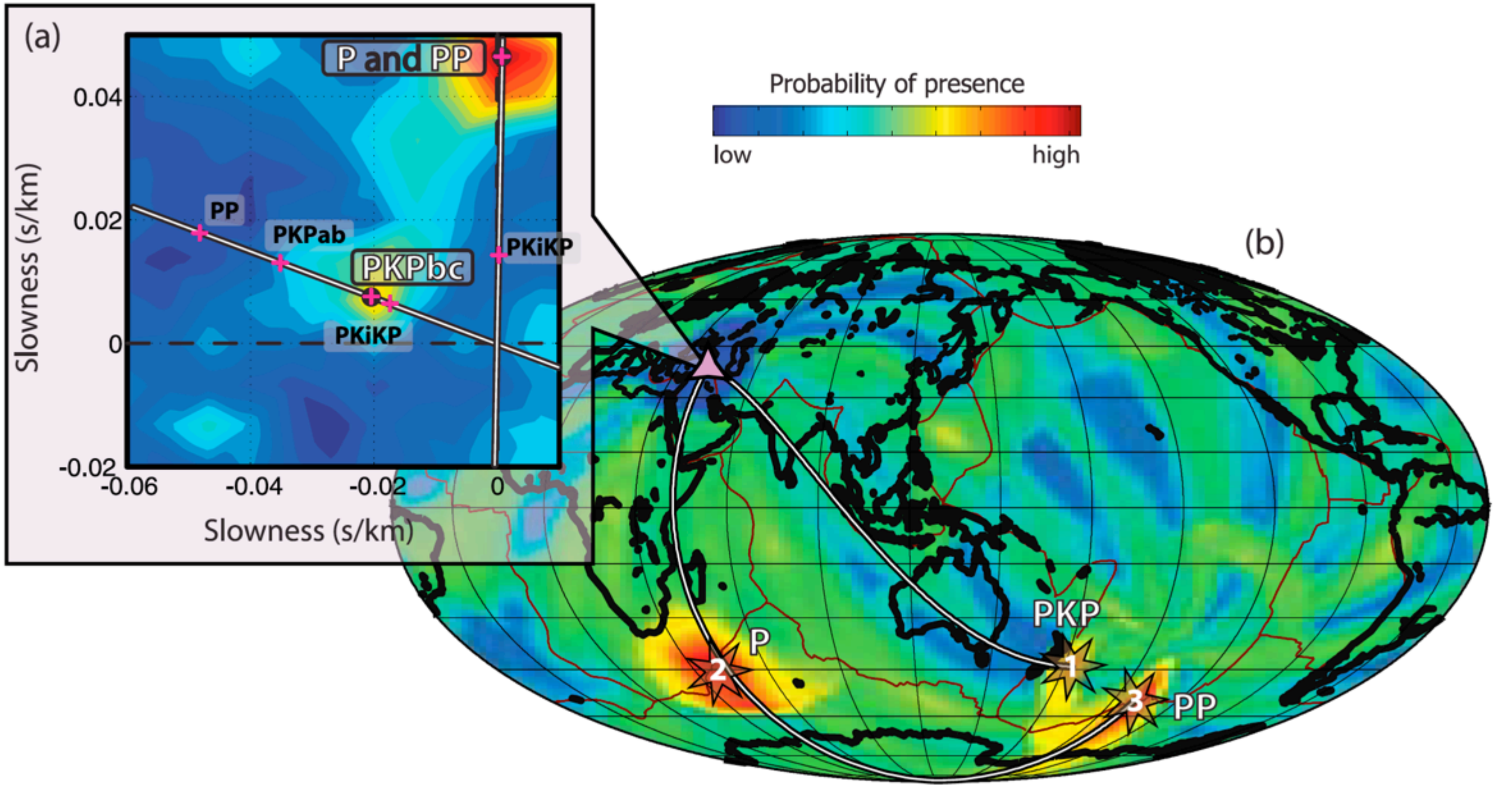

POLENET/LAPNET array

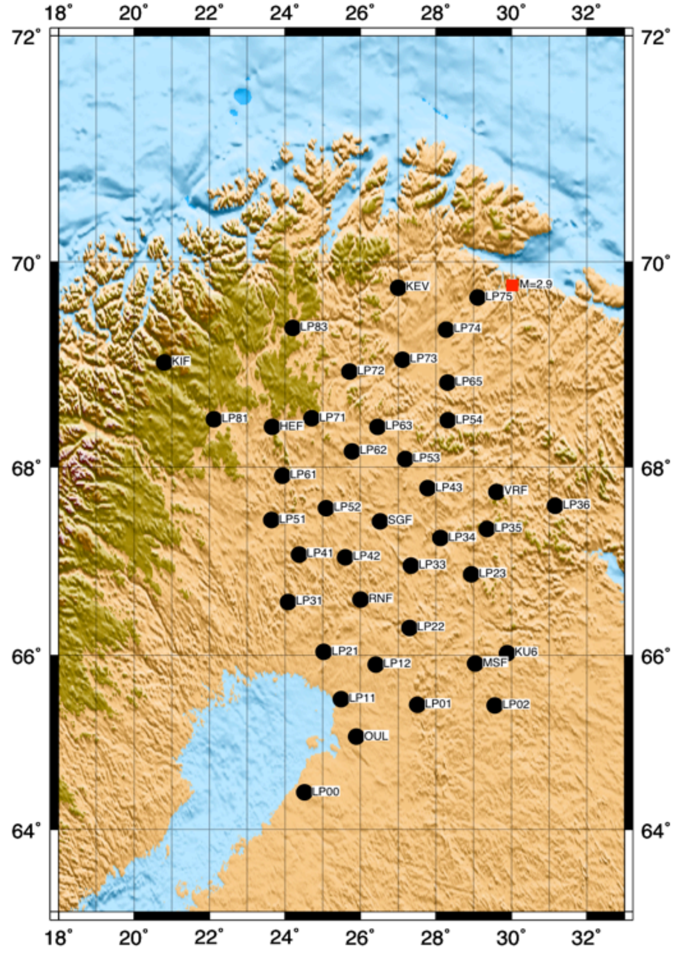

➔Earth’s mantle discontinuities from ambient seismic noise (crystalline phase transition ➔ (P,T))

Poli et al. Science 2012

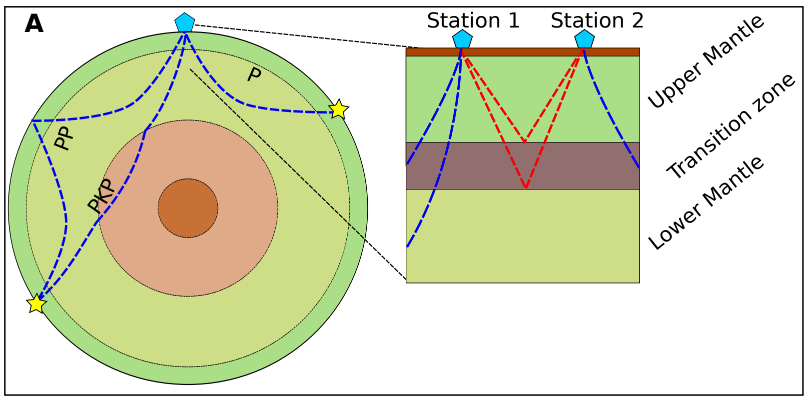

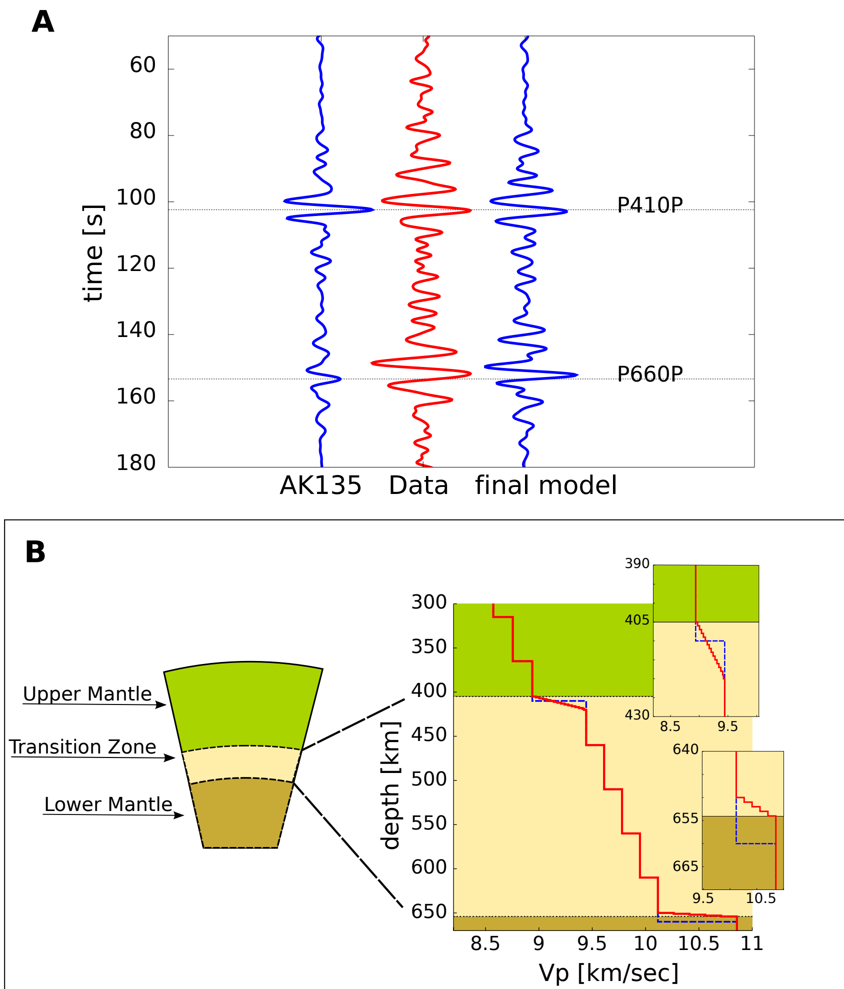

GLOBAL TELESEISMIC CORRELATIONS (periods 25-100s)

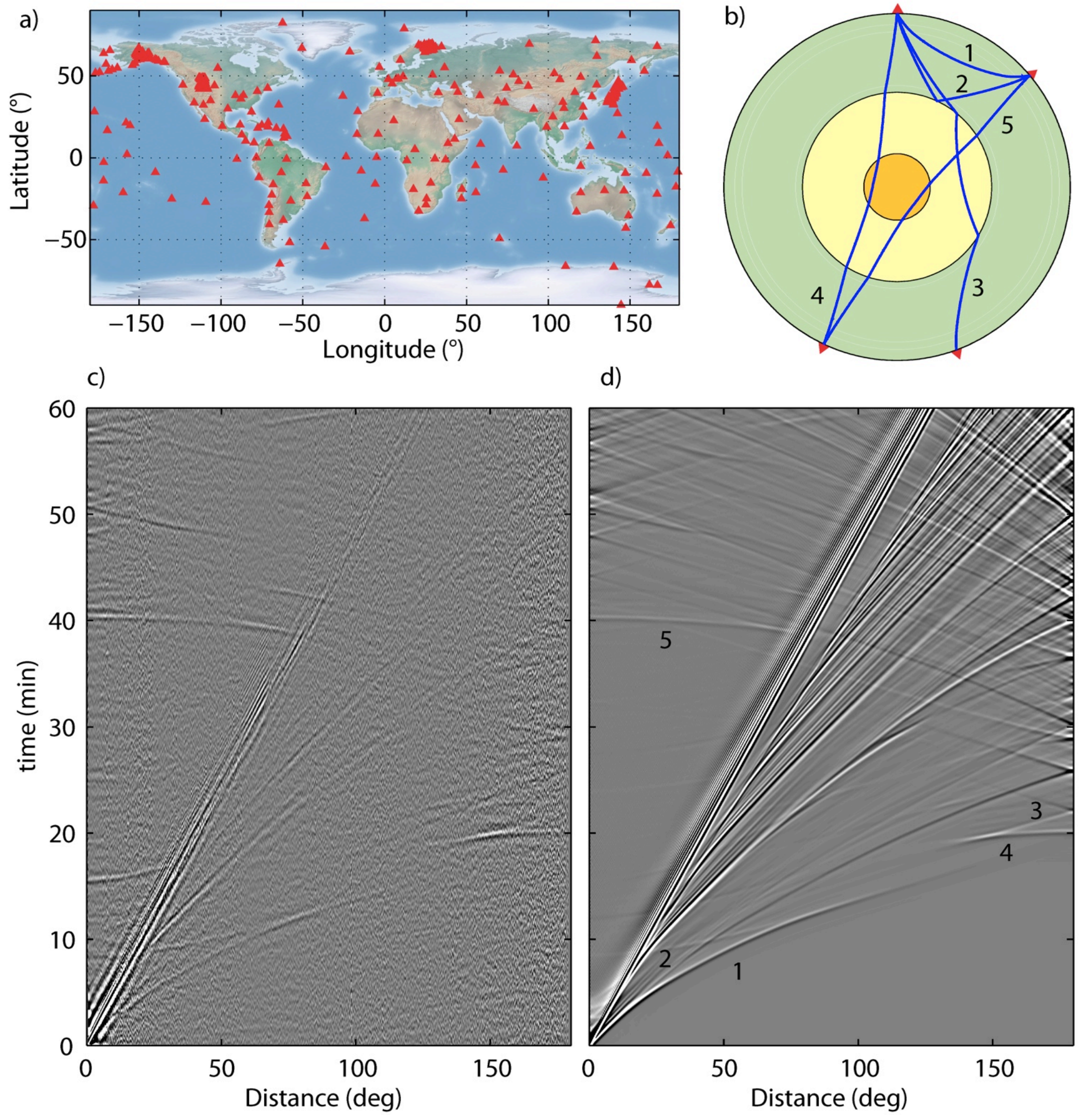

Boué, Poli et al., GJI 2013

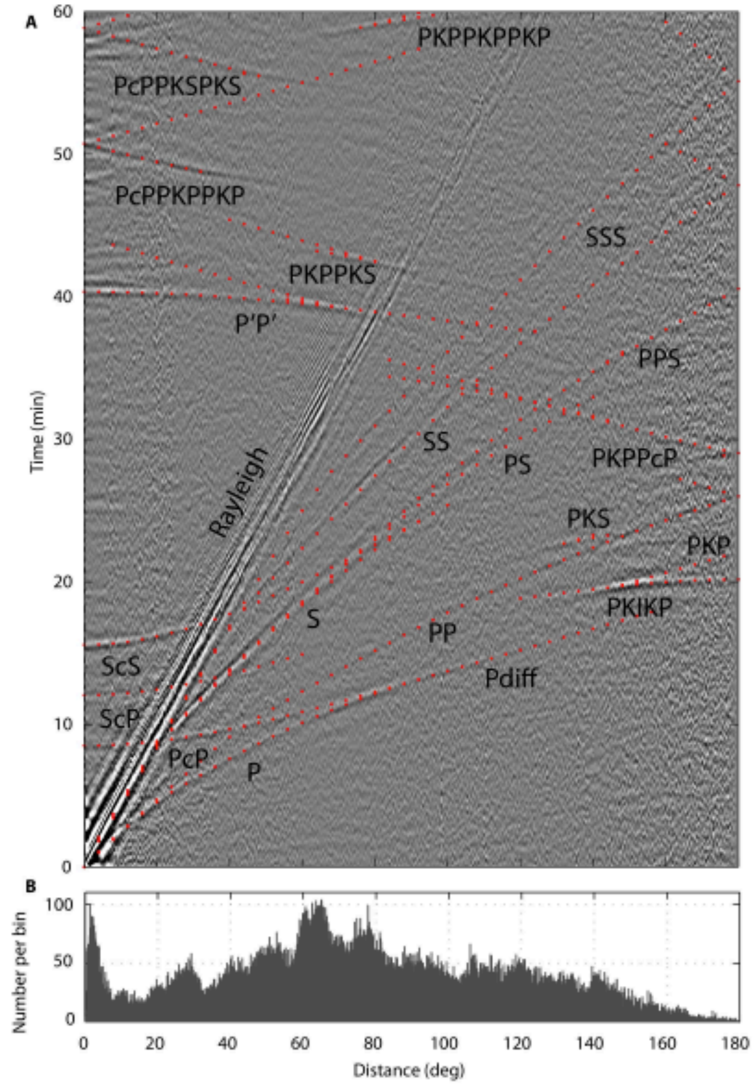
A
PKPPKPPKP
PcPPKSPKS
PcPPKPPKP
SSS
PKPPKS
P'P'
PPS
Rayleigh
SS
PS
PKPPcP
PKS
PKP
PKIKP
S
PP
ScS
Pdiff
ScP
PcP
P
Time (min)
B
Number per bin
Distance (deg)

Periods 5-10s

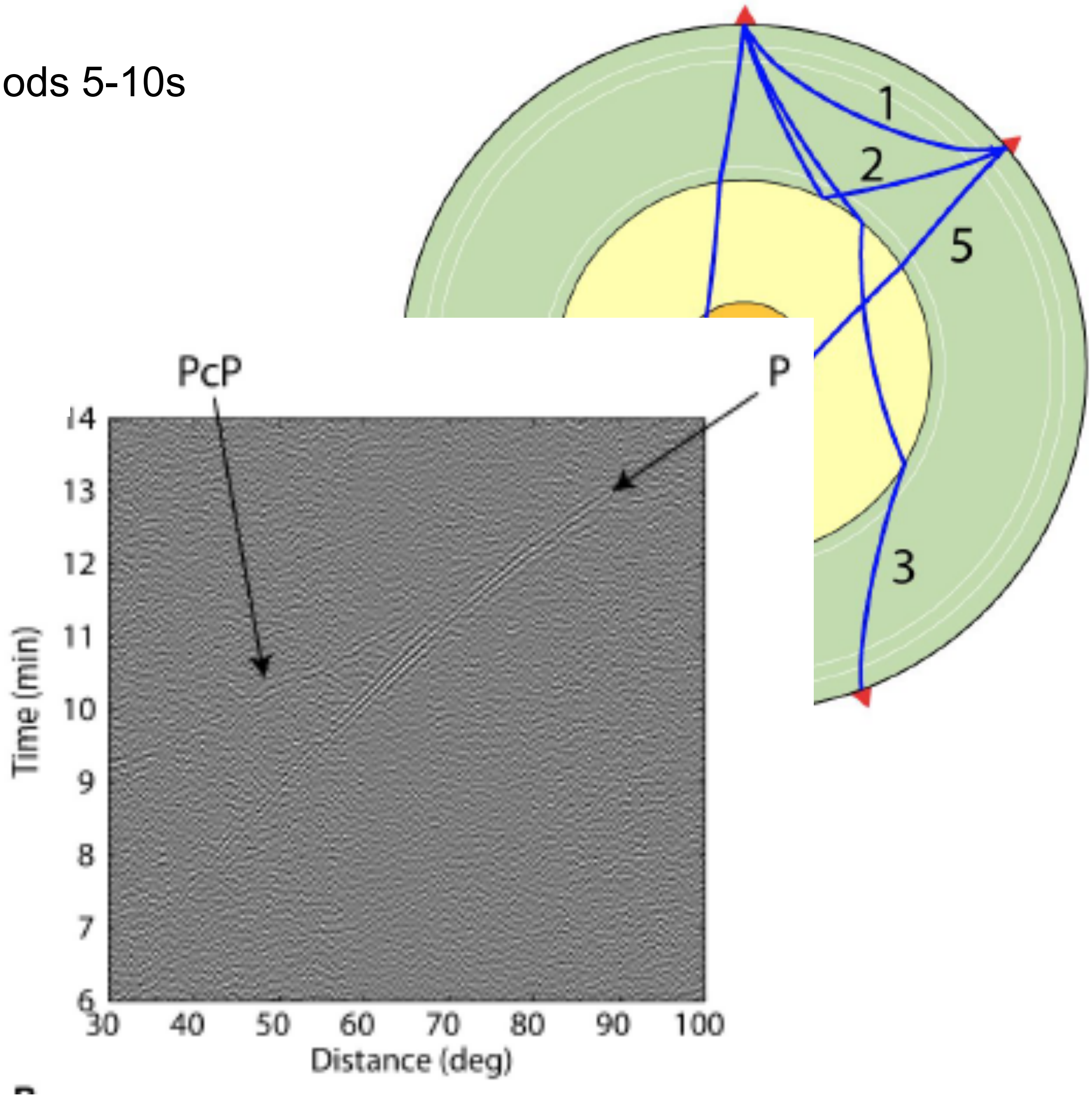

Application to tomography
Yellowstone anomaly

Comparison of teleseismic correlations (Finland-US) with tomographic model expectation

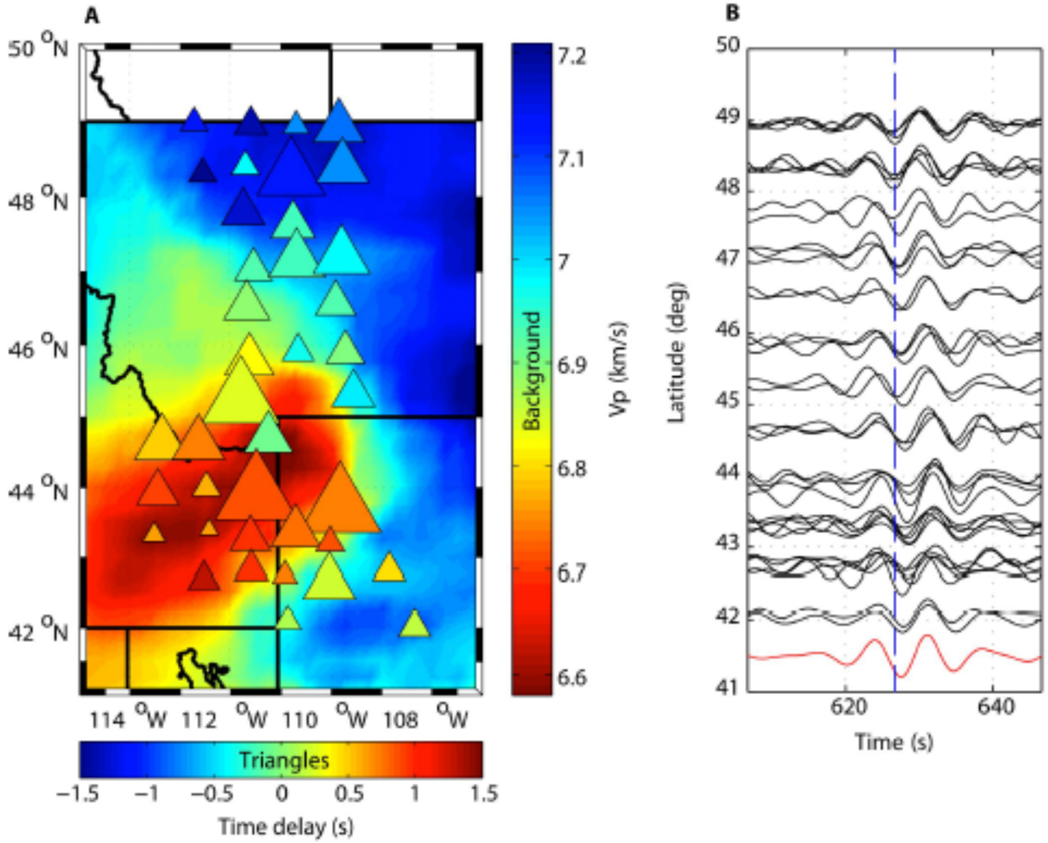

Boué, Poli et al., GJI 2013

Measure of the anisotropy of the inner core:
(polar paths are faster than equatorial paths)

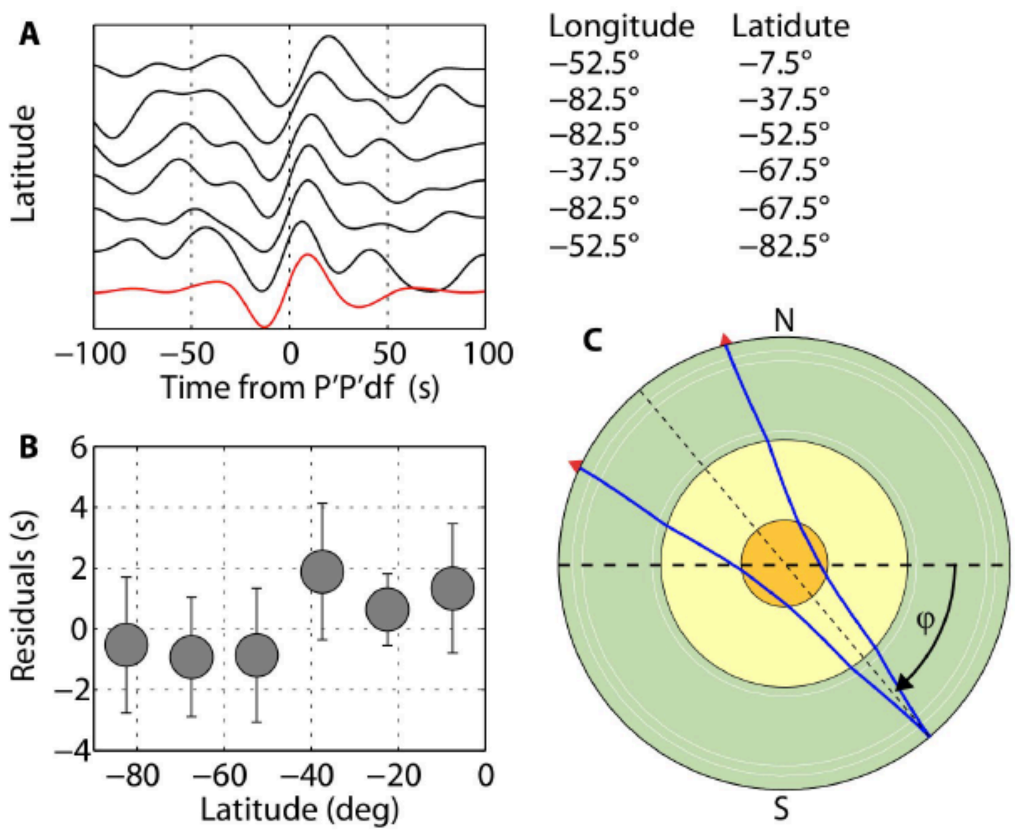

Boué, Poli et al., GJI 2013

➔ Numerous applications to come!

-Introduction

-Passive imaging

-**Monitoring the changing Earth**

Structural monitoring: talks by P. Gueguen and M. Todarovska

Correlation functions as approximate Green functions
(ex: period band:2-8s Parkfield, Brenguier et al., 2008)

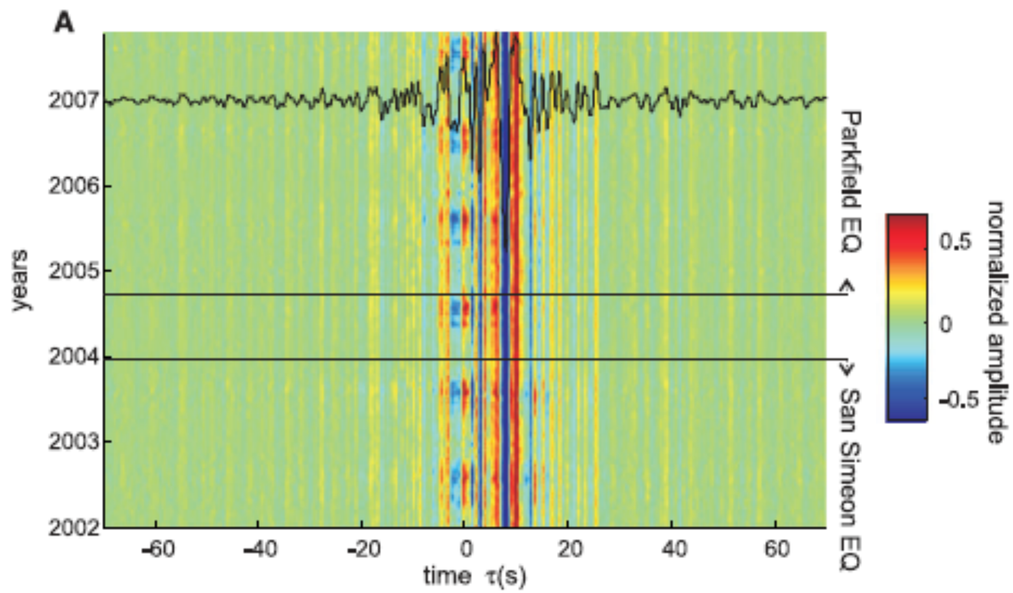

Direct waves are sensitive to noise source distribution (errors small enough for tomography (≤1%) but too large for monitoring (goal ≈ 10^{-4})

Stability of the ‘coda’ of the noise correlations = frozen distribution of scatterers

We can construct virtual seismograms between stations pairs from noise records.

They contain the information about structures, but also all the complexity of actual seismograms

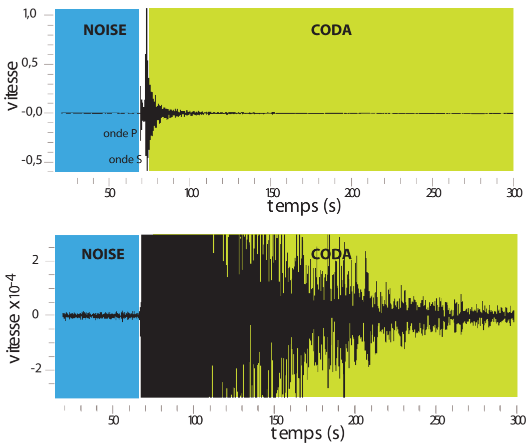

Specifically they contain the scattered waves (coda waves). This is attested by the fact that we can also construct ‘virtual’ seismograms from the correlation of noise based virtual seismograms

➔ C^3 method *(Stehly et al., 2008; Garnier et al., 2011)*

➔ can even be iterated in C^5.. *(Froment et al., 2011)*

➔ long travel times = strong sensitivity to changes

Illustration of C3

(a) Computation of noise correlations (virtual seismograms)

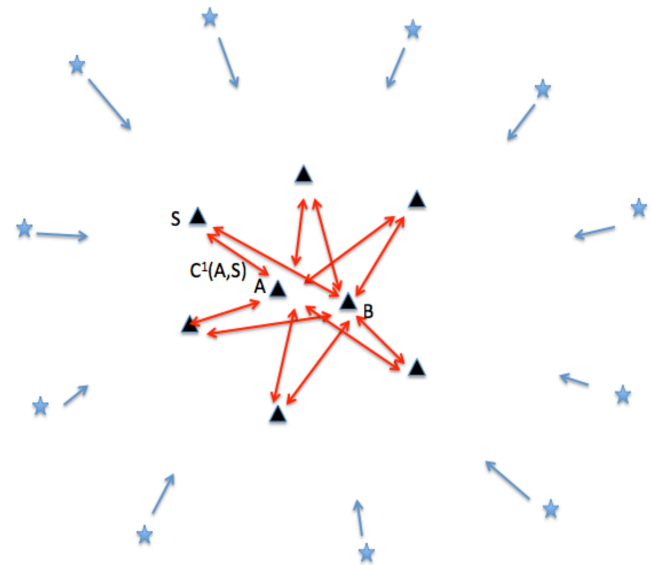

(b) Correlations of noise correlation codas (stations as virtual sources)

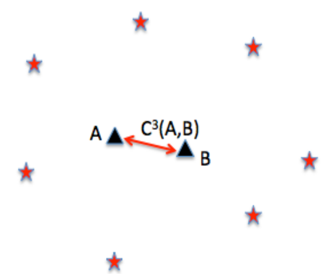

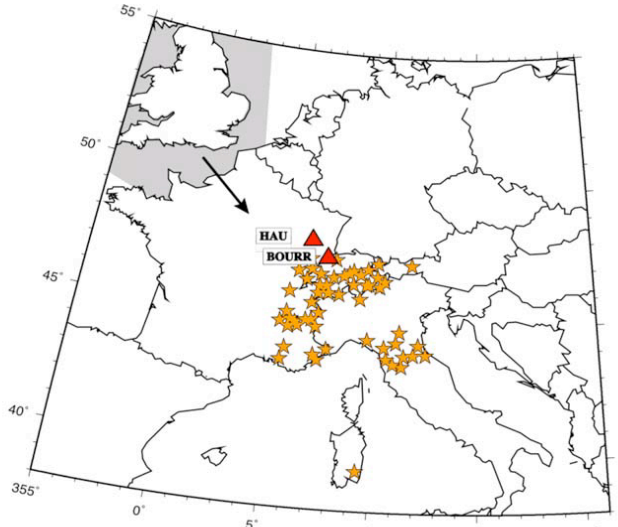

55°
50°
45°
40°
355°
0°
5°
10°
15°
20°
HAU
BOURR

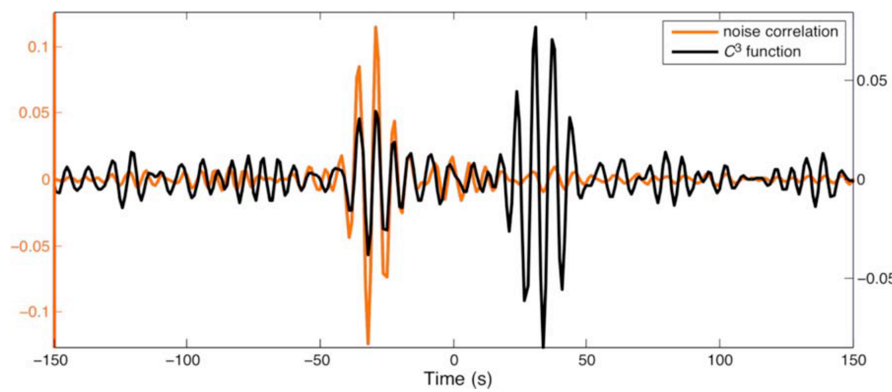

noise correlation
C^3 function
0.1
0.05
0
−0.05
−0.1
0.05
0
−0.05
−150
−100
−50
0
50
100
150
Time (s)

Detecting a small change of seismic speed: coda waves

Comparing a trace with a reference under the assumption of an homogeneous change

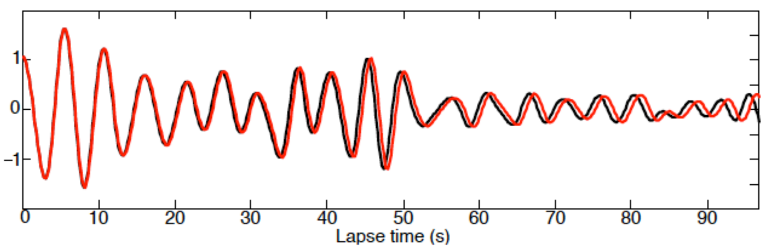

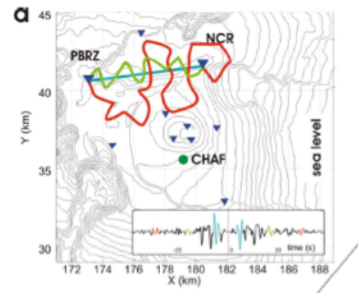

The ‘doublet’ method: moving window cross spectral analysis

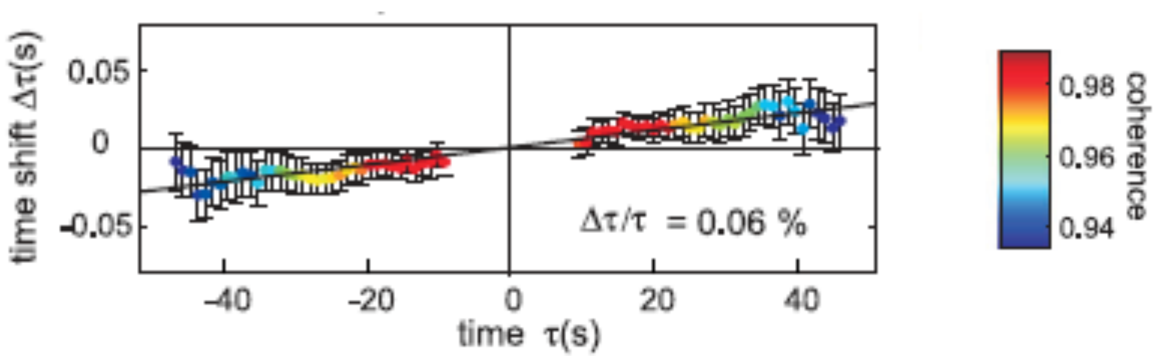

Alternative technique: stretching

Surface effects

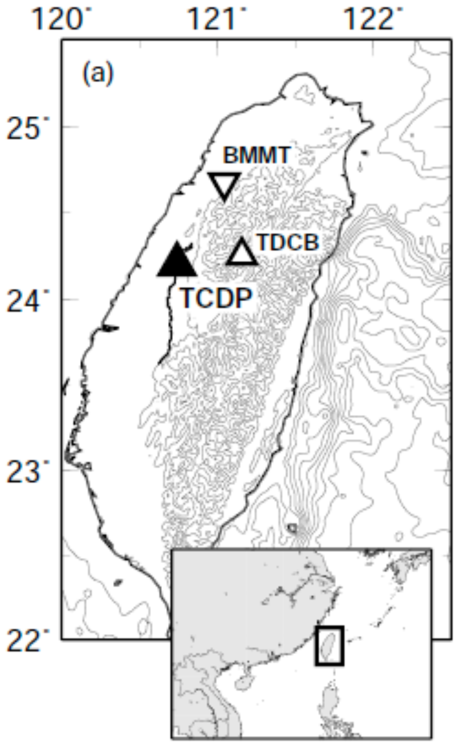

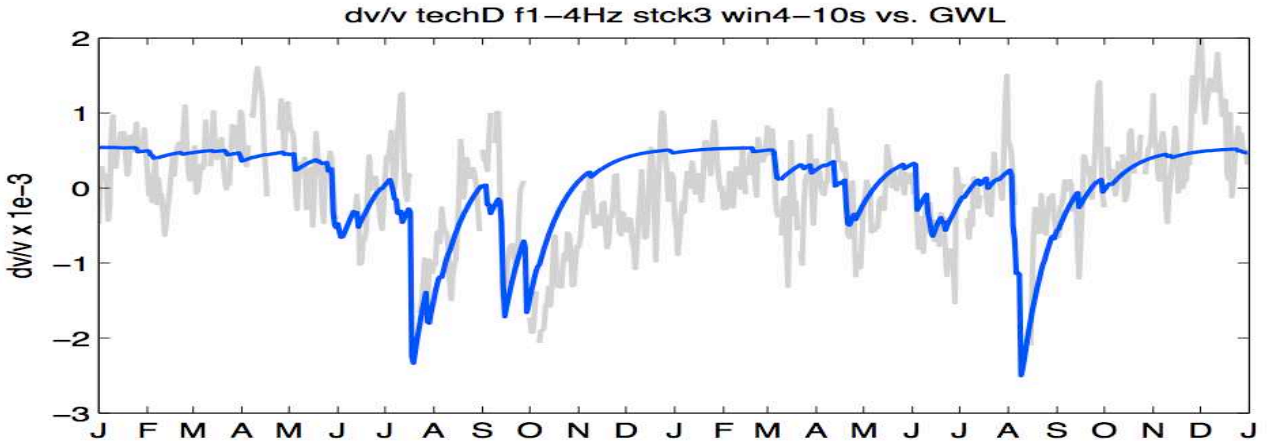

grey: variations of seismic speed

blue: model of the effet to the level of water table deduced from meteorological data

Seismic speed changes before the eruptions…

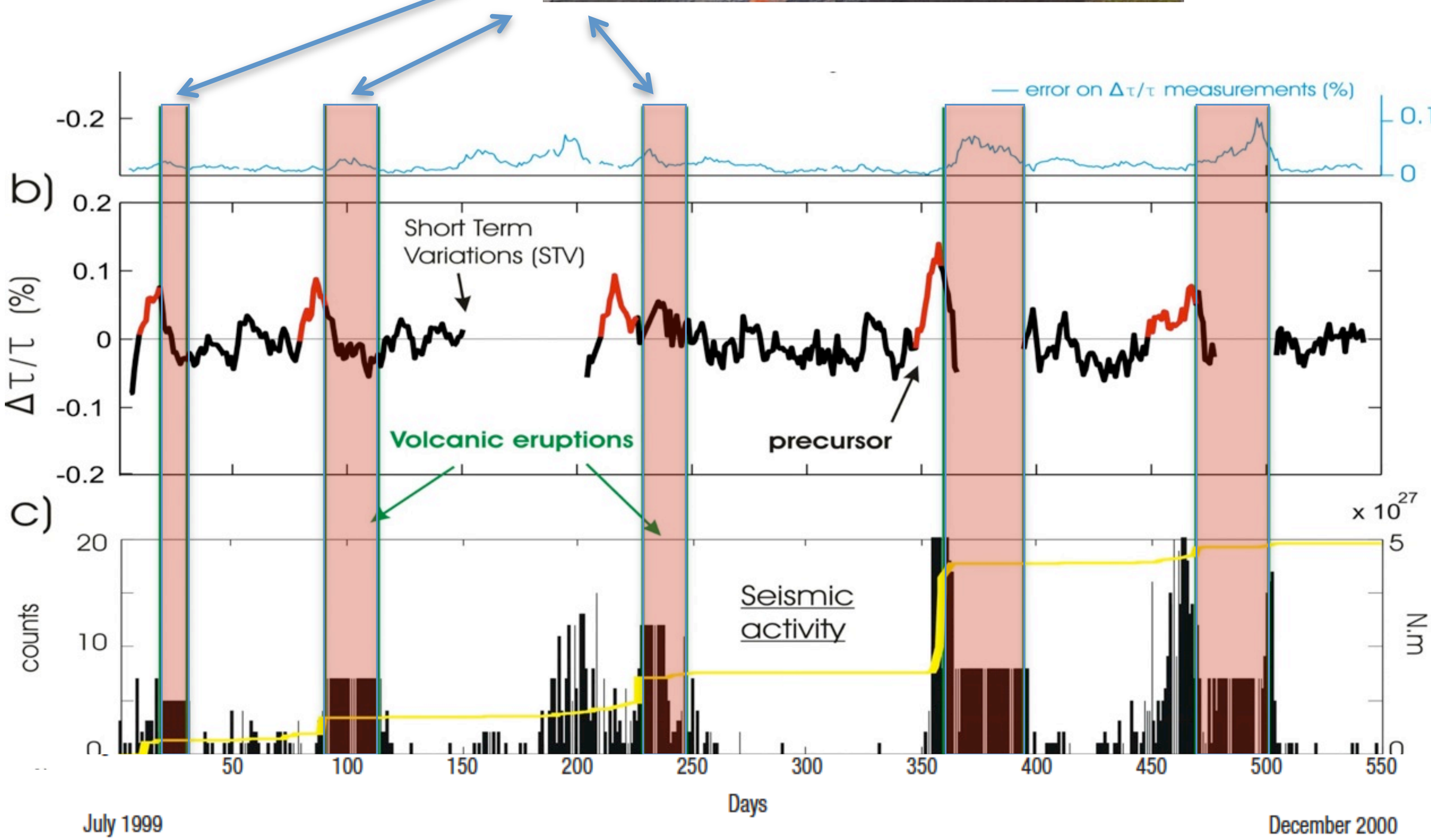

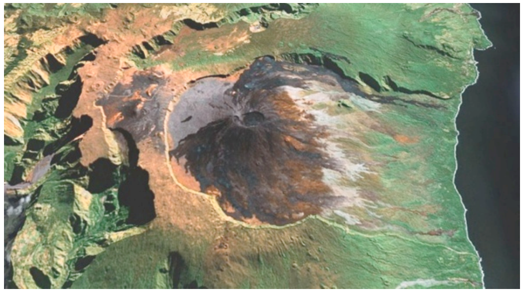

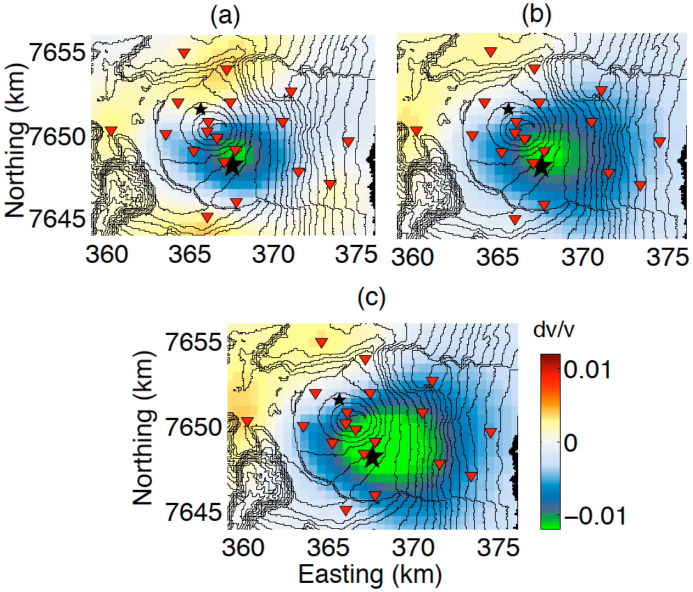

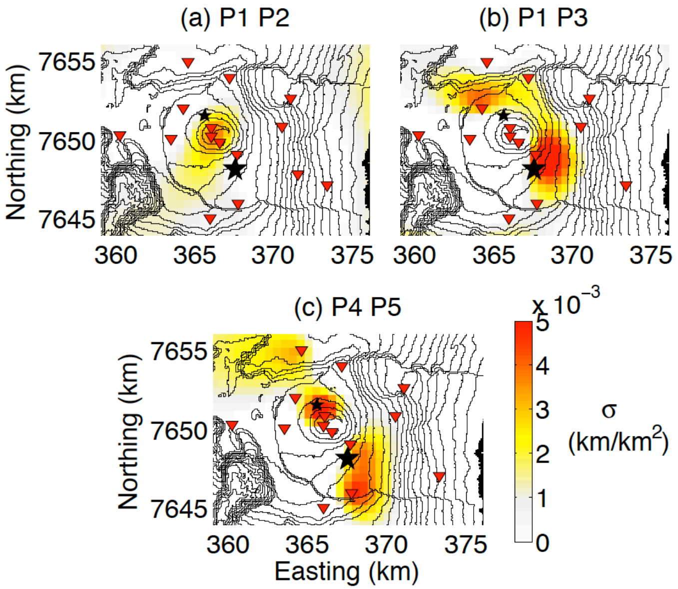

Local change of speed

Local change of scattering properties

Anne Obermann PhD 2013

(discussed by E. Larose and F. Brenguier)

Application to Parkfield *(Brenguier et al. 2008)*
Short period sensors / Processing in the period 1-10s

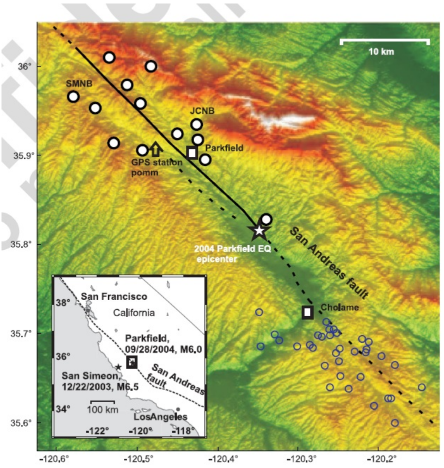

HRSN network

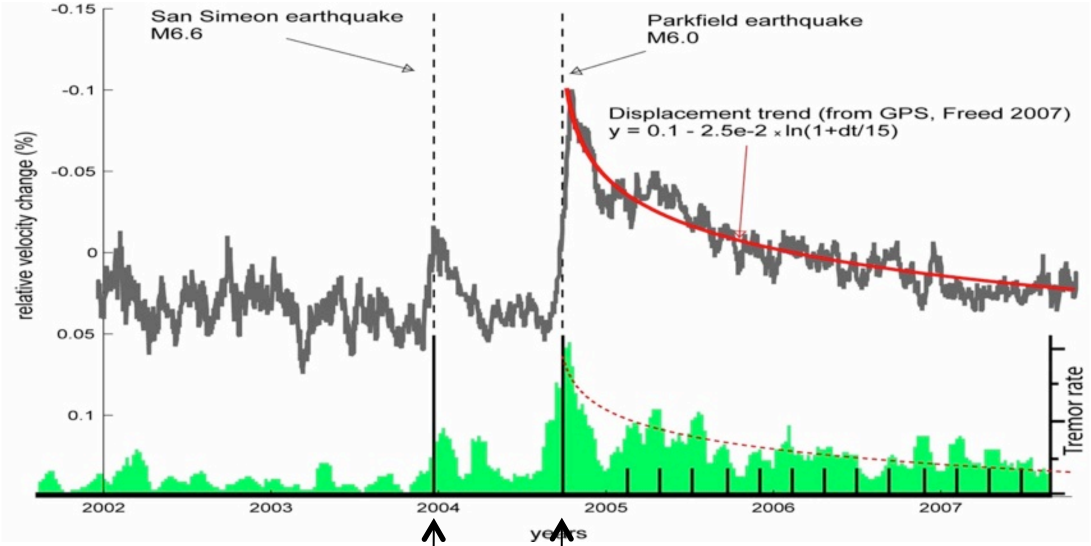

Distant event **Local event**

(Talks by P. Johnson and Y. Ben-Zion)

➔ GPS trend
➔ tremor activity
➔ but ambiguity with non-linear effect of strong ground motion on surficial materials

‘Silent’ event of slip on the Subduction plane (40km deep)

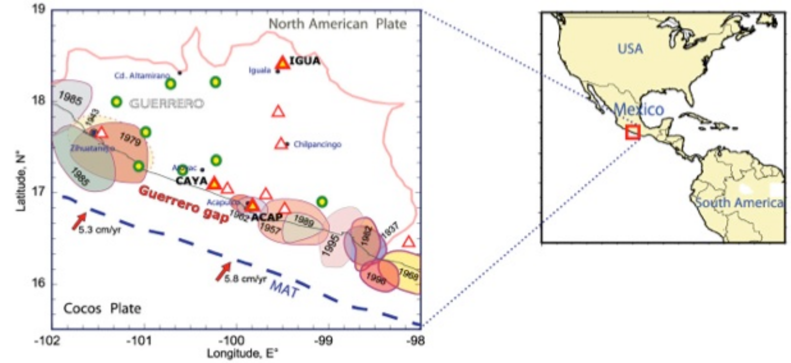

GPS motion towards the North during interseismic periods (NO significants events)

Mw7.6

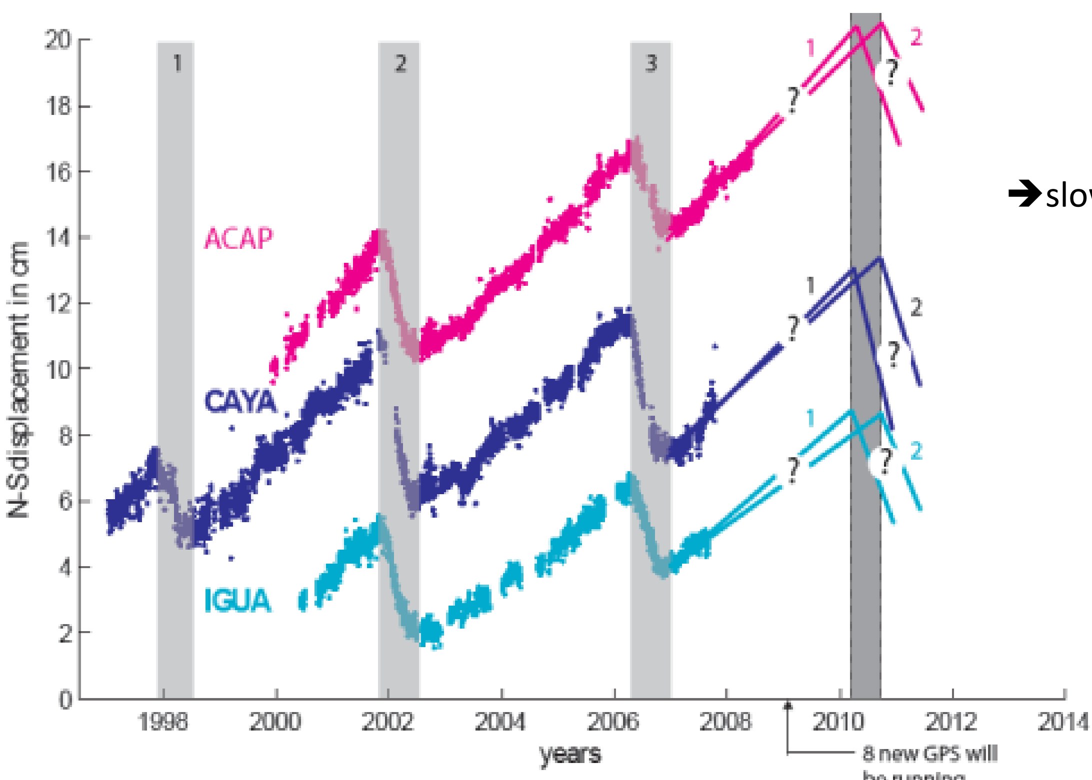

➔slow slip events (SSEs)

(Cotte et al., 2009)

Temporal relation between velocity change and dilatation

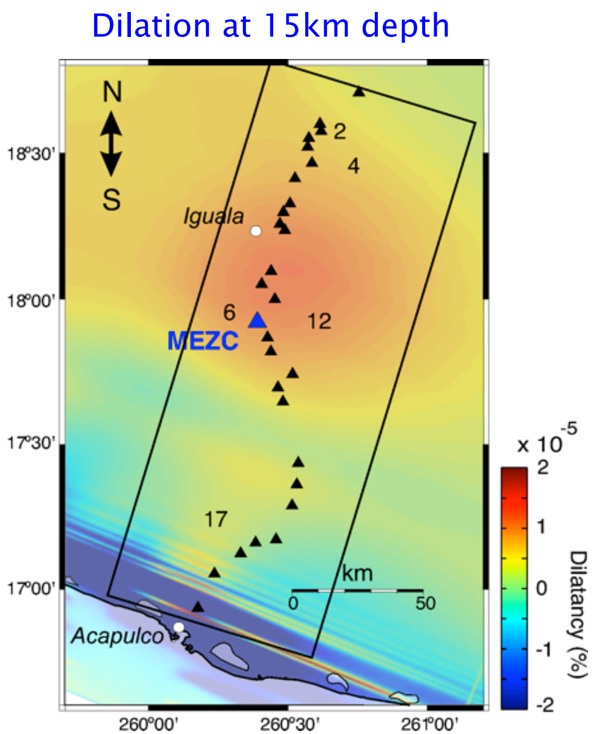

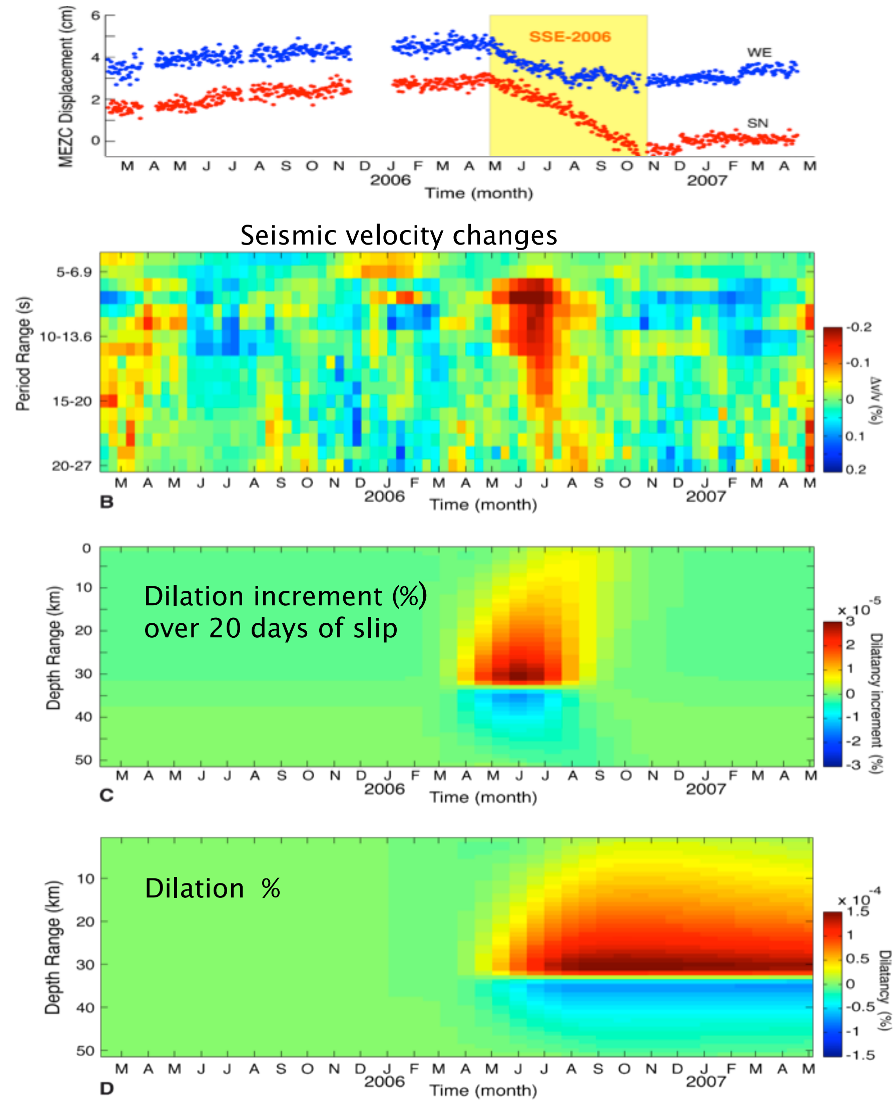

- The minimum of velocity and maximum of dilation rate produced by the SSE occurs in June 2006
- The dilation and the velocity perturbation affect the volume and are not localized at the surface

Rivet et al., 2011

2009-2010 Slow Slip Event

Apparent temporal change of velocity (t,T)

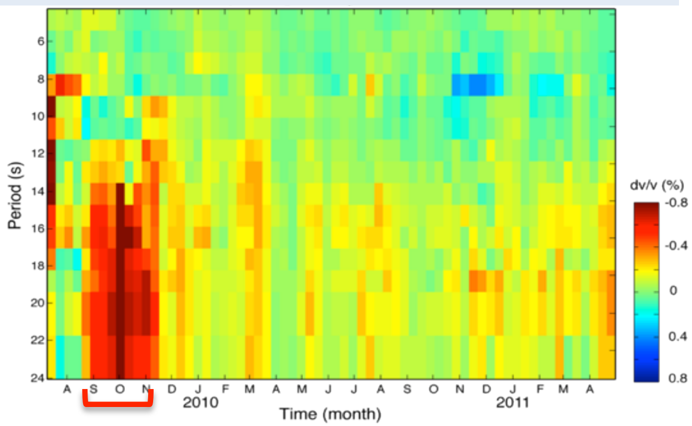

Linearized Rayleigh wave inversion

Resolution matrix

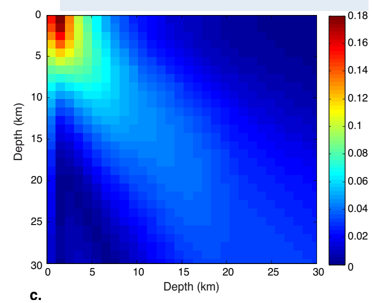

Monte Carlo inversion

With the period band available, we conclude that the change occurs in the lower crust or below.

Temporal change of velocity (t,z)

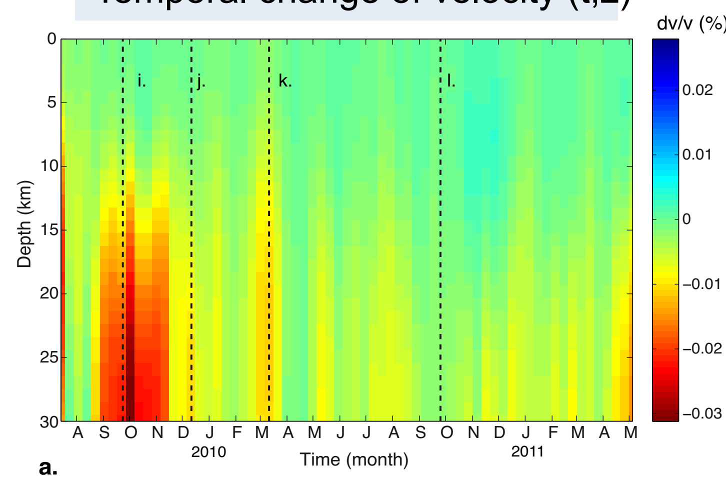

Rivet et al., 2012